Excited-state non-adiabatic dynamics simulations of pyrrole

Hans Lischka, Mario Barbatti, Mario Vazdar, Mirjana Eckert-Maksic

▶ **To cite this version:**

Hans Lischka, Mario Barbatti, Mario Vazdar, Mirjana Eckert-Maksic. Excited-state non-adiabatic dynamics simulations of pyrrole. Molecular Physics, 2009, 107 (08-12), pp.845-854. 10.1080/00268970802665639 . hal-00513244

HAL Id: hal-00513244
https://hal.science/hal-00513244

Submitted on 1 Sep 2010

HAL is a multi-disciplinary open access archive for the deposit and dissemination of scientific research documents, whether they are published or not. The documents may come from teaching and research institutions in France or abroad, or from public or private research centers.

L'archive ouverte pluridisciplinaire **HAL**, est destinée au dépôt et à la diffusion de documents scientifiques de niveau recherche, publiés ou non, émanant des établissements d'enseignement et de recherche français ou étrangers, des laboratoires publics ou privés.

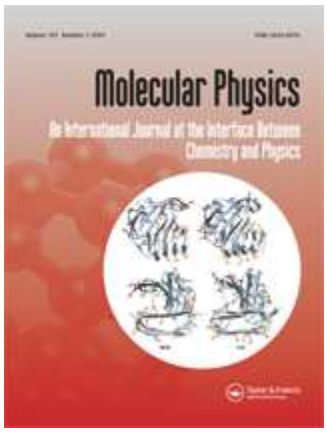

Excited-state non-adiabatic dynamics simulations of pyrrole

Journal:	*Molecular Physics*
Manuscript ID:	TMPH-2008-0381.R1
Manuscript Type:	Special Issue Paper - Fritz Schaefer
Date Submitted by the Author:	27-Nov-2008
Complete List of Authors:	Lischka, Hans; University of Vienna, Institute for theoretical Chemistry Barbatti, Mario; University of Vienna, Institute for Theoretical Chemistry Vazdar, Mario; Rudjer Bošković Institute Eckert-Maksic, Mirjana; Rudjer Bošković Institute
Keywords:	non-adiabatic dynamics, conical intersection, photochemistry

scholarONE™
Manuscript Central

Excited-state non-adiabatic dynamics simulations of pyrrole

Mario Vazdar,[a] Mirjana Eckert-Maksić,[a*] Mario Barbatti,[b*] Hans Lischka[b*]

[a] *Laboratory for Physical-Organic Chemistry – Division of Organic Chemistry and Biochemistry. Rudjer Bošković Institute, 10002 Zagreb, Croatia;* [b] *Institute for Theoretical Chemistry – University of Vienna, Waehringerstrasse 17, A 1090 Vienna, Austria.*

For Peer Review Only

Abstract

Non-adiabatic on-the-fly-dynamics simulations of the photodynamics of pyrrole were performed at multireference configuration interaction level involving five electronic states with a simulation time of 200 fs. The analysis of the time dependence of the average state occupations shows that the deactivation of pyrrole to the electronic ground state takes place in about 140 fs. This deactivation time agrees very well with the experimentally measured time constant of 110 fs for the formation of fast hydrogen atoms. After excitation into the S_4 state, 80% of the trajectories followed the NH-stretching mechanism giving rise to a population of fast H atoms. The computed average kinetic energy is in good accord with the experimentally observed average kinetic energy of the fast hydrogen atoms. It is found that 10% of trajectories followed the ring-puckering mechanism and 3% followed the ring-opening mechanism. This latter mechanism was characterized in pyrrole for the first time and involves the conical intersection of lowest energy of this molecule.

Keywords: non-adiabatic dynamics; conical intersection; photochemistry; pyrrole

* Corresponding authors: H. Lischka (hans.lischka@univie.ac.at), M. Barbatti (mario.barbatti@univie.ac.at) and M. Eckert-Maksić (mmaksic@emma.irb.hr)

1. Introduction

Pyrrole is one of the simplest biologically relevant heteroaromatic compounds. For this reason, its electronic states have been intensively studied both experimentally and theoretically during the last decades with the emphasis on its UV spectrum [1-10] and its photodynamics [11-24]. In particular, it is known that the deactivation of UV-excited pyrrole to the ground state occurs at a very short (femtosecond) time scale [19] with low luminescence quantum yields [25], indicating the dominance of internal conversion processes. Sobolewski and coworkers [13] have proposed that the deactivation of pyrrole and related heteroatomic compounds occurs via the NH-stretching mechanism along a $^1\pi\sigma_{NH}^*$ repulsive state. This mechanism, which has been examined in detail [15, 16, 22, 23] by means of wave packet dynamics simulations, can fully explain the presence of fast H atoms in the photofragmentation spectra [26]. Nevertheless, the mechanism responsible for the formation of slow H atoms and of other experimentally observed fragments such as HCN and CNH_2 [11, 14, 17, 19, 20] is still subject of considerable debate [15, 19, 26-28].

Recently, we have suggested [27] that non-adiabatic deactivation of pyrrole may also proceed via a ring-puckering mechanism. This second kind of mechanism could not only be the source of heavy fragments, but also partially explain the slow H atoms [29]. Also recently, a third deactivation mechanism that can be relevant for pyrrole was identified in thiophene [30], furan [31], imidazole [32], and in the imidazole group of adenine [33]. In this mechanism the deactivation of five-membered rings proceeds by a planar ring-opening deformation. This process was observed to occur in a minor fraction of trajectories during dynamics simulations of adenine [34]. Based on these findings, we have currently attempted and succeeded to locate this type of mechanism in pyrrole, too.

For Peer Review Only

Profant *et al*. [35] and Poterya *et al.* [28] have experimentally investigated the photolysis of pyrrole clusters. In addition, they have also performed theoretical calculations on the isolated pyrrole and on pyrrole complexes [28]. They have found that in presence of solvent molecules the NH stretching mechanism is inhibited, which results in a strong reduction of the fast H atom elimination process while keeping the slow H atom elimination. These are important results that on one hand once more confirm the role of the NH-stretching mechanism for the fast H atoms formation and on the other hand indicate that ring deformation mechanisms should be involved in the slow H atoms formation.

The strong dependence of different fragment yields on the excitation energy [26] indicates that the individual mechanisms are in mutual competition and can play different roles depending on the initial conditions. Excited-state energy surfaces have been investigated in detail under special consideration of crossings between different energy surfaces as already mentioned above [1, 18, 23, 27, 28, 36] and reaction paths have been constructed subsequently. This information led to substantial progress in the understanding of the photochemical processes in pyrrole. However, it turned out to be very difficult to estimate the importance of individual intersections and related reaction pathways. In order to better understand how these mechanisms are activated, it is desirable to perform dynamics simulations. Such simulations exhibit a substantial complexity. For instance, as for selecting the proper quantum chemical methods, it needs to be taken into account that: first, the non-adiabatic dynamics of pyrrole involves multiple excited states showing often multireference character and, secondly, that it is essentially impossible to identify just a few important internal degrees of freedom by which the photochemical reaction mechanism can be described. Therefore, an essential condition is the usage of the full set of nuclear coordinates. These are usual requirements to be met e.g. in simulations of organic chromophores exhibiting high density of excited states [34, 37, 38]. One convenient way to satisfy especially

URL: http://mc.manuscriptcentral.com/tandf/tmph

For Peer Review Only

the second condition is to use mixed-quantum classical dynamics methods [39-44]. In this work surface hopping dynamics is performed using the fewest-switches algorithm of Tully [45]. The advantage of this approach is that it allows the application of an "on-the-fly" strategy [42, 43, 46] where a pre-selection of certain internal degrees of freedom and any fitting of pre-computed potential energy points is avoided by computing at each time step the energies, the complete energy gradient and non-adiabatic coupling terms required for the integration of Newton's equations of motion and the time-dependent Schrödinger equation. This on-the-fly strategy is computationally very expensive and requires analytical energy gradients and non-adiabatic coupling vectors for computational efficiency. Due to the stringent computational requirements most of the photodynamical simulations have been performed so far at the relatively cost-effective complete active space self consistent field level (CASSCF). Since in this case dynamical electron correlation effects are mostly neglected, the relative balance of electronic states of different character can be strongly violated. It should be stressed that the non-adiabatic dynamics simulations presented here were carried out at a significantly higher level using the MR-CISD method including five electronic states. This represents the state-of-the-art approach for this kind of simulations, which has not been documented before for molecules of the size of pyrrole to the best of our knowledge. The present calculations have been made possible by use of the analytic gradient features of the program package COLUMBUS [47-49] as it will be described below.

2. Computational details

Multireference configuration interaction (MRCI) and complete active space self-consistent field (CASSCF) calculations were performed for pyrrole. The CAS space was comprised of four π electrons in five orbitals (two π orbitals, two π* orbitals and one Rydberg 3s orbital). This space will be conventionally designated as CAS(4,5) in the text. State averaging was

URL: http://mc.manuscriptcentral.com/tandf/tmph

For Peer Review Only

performed over five singlet states with equal weights (ground state, two valence ππ* states and two Rydberg π3s states), which will be denoted as SA-5. MRCI calculations were performed based on the orbitals computed by the SA-5-CASSCF(4,5) wave function. The reference configurations for the MRCI were constructed within the CAS(4,5) by allowing single and double excitations from the two π orbitals into the two π* orbitals and the Rydberg 3s orbital. The final configuration space was constructed by allowing all single and double excitations from the reference configurations into the virtual orbital space (MR-CISD). All core electrons and the lowest eight additional orbitals were frozen in the MRCI calculations and the interacting space restriction [50] was applied. The basis set was composed of aug'-cc-pVDZ type [51] on the nitrogen and carbon atoms (the prime indicates that d-aug functions were removed). On the hydrogen atom connected to nitrogen, the cc-pVDZ basis set was used, whereas for the remaining hydrogen atoms the cc'-pVDZ basis set was used (the prime signifies that p-functions were deleted). This hybrid basis set will be denoted as BS.

The MRCI approach and the basis set were selected by balancing the accuracy requirements of the calculations of four excited states of different character (see Table 1) and the need for computational efficiency, since an on-the-fly approach requires several tens of thousands of individual MRCI calculations to be carried out. Therefore, before starting the dynamics simulations an extensive set of calculations had been performed, including the Franck-Condon region, the seam of conical intersections, and reaction pathways. For the determination of minima on the crossing seam (MXS), starting geometries were selected from our previous MRCI calculations on pyrrole [27] and were reoptimized with the above-described MRCI method. Reaction paths for the two ring-deformation processes were constructed by the method of linear interpolation of internal coordinates (LIIC) between the ground-state geometry and the corresponding ring-deformed conical intersections. The reaction path for the NH-stretching process was constructed by rigidly stretching the NH

URL: http://mc.manuscriptcentral.com/tandf/tmph

For Peer Review Only

distance in steps of 0.2 Å starting from the ground state equilibrium structure up to a NH distance of 2.6 Å.

All energy calculations and MXS optimizations were performed by using analytical gradient and non-adiabatic coupling procedures described in References [52-56]. For vertical excitation energy calculations, the Davidson correction (+Q) [53, 57, 58] was used in order to describe higher order excitation effects. For the C_{2v} labeling of the states, the *x* axis was assumed to be oriented perpendicular to the ring plane.

Mixed quantum-classical dynamics calculations were performed for pyrrole by using an on-the-fly approach [42, 43, 46, 59, 60]. Energies, gradients, and non-adiabatic coupling vectors were computed at each time step at the MR-CISD/SA-5-CASSCF(4,5)/BS level of theory. The nuclear motion was represented by classical trajectories computed by numerical integration of Newton's equations by the velocity-Verlet algorithm [61]. Non-adiabatic effects were taken into account by means of the surface hopping approach [45]. Time-dependent adiabatic populations were corrected for decoherence effects [62] (α = 0.1 hartree) and used to calculate surface hopping probabilities in accordance to the Tully's fewest switches approach [45]. In order to alleviate the computational costs, no coupling vectors were calculated between non-consecutive states [44]. In total, 90 trajectories were computed. The initial Cartesian coordinates and momenta were selected from a quantum harmonic oscillator (Wigner) distribution in the ground state. The trajectories were started in the S_4 state at these geometries. This procedure gave rise to a composition of 60% of trajectories initially in the $\pi\pi^*$ states and 40% in the $\pi 3s/\pi\sigma_{NH}^*$ states. The minimum excitation energy was 6.36 eV while the average was 6.76 eV with a standard deviation of 0.26 eV. The trajectories were then propagated for a maximum time of 200 fs with a time step of 0.5 fs.

The structures of the puckered geometries were described in terms of the Cremer-Pople parameters Q and ϕ [63]. While the parameter Q measures the extent of puckering (Q =

For Peer Review Only

0 Å indicates a planar structure), the parameter ϕ describes the kind of puckering. For 5-mebered rings, there are only few kinds of puckered conformations available: envelope conformations with atom *k* above (^{k}E) or below (E$_{k}$) the ring plane and twisted conformations with atom *k* above the ring plane and atom *k*-1 below the ring plane (^{k}T$_{k-1}$). Because of the pyrrole symmetry, ϕ can be reduced to the 0° – 90° range by projecting all values on this quadrant.

All CASSCF and MR-CISD+Q calculations were performed with the COLUMBUS [47-49] program package. The atomic orbital (AO) integrals and AO gradient integrals have been calculated with program modules taken from DALTON [64]. The dynamic simulations were carried out using the NEWTON-X program [42, 65] with an interface to the COLUMBUS program package.

Table 1. (around here)

3. Analysis of the energy surfaces

In order to investigate the reliability of the MRCI method used in the dynamics study, we have performed a series of tests and comparisons with other previously published results. Specifically, we have compared vertical excitation energies, reaction paths, and MXS structures with results obtained with methods of higher level of theory.

3.1 Vertical excitation energies

The theoretical computation of vertical excitation energies of pyrrole and the assignment of the experimental UV spectrum have been a matter of discussion for a long period of time [1, 3, 4, 8, 9]. The currently calculated values are compared to other available theoretical and experimental results in Table 1. The comparison reveals that vertical excitation energies computed by the MR-CISD/SA-5-CASSCF(4,5)/BS method are in good accordance with

URL: http://mc.manuscriptcentral.com/tandf/tmph

For Peer Review Only

results obtained previously by the MR-CISD+Q/SA-5-CAS(6,5)+AUX(1)/d-aug-cc-pVDZ method [27] where the auxiliary (AUX) orbital represents the 3s Rydberg orbital into which single excitations from the valence CAS(6,5) are allowed. Most of the calculated vertical excitation energies differ by ca. 0.1-0.2 eV, except in the case of the $^1B_1$ state where this difference is 0.35 eV. Furthermore, the present results for the $^1A_2$ and $^1B_1$ Rydberg states are in excellent agreement with experimental values assigned in Ref. [9]. The current energies of the ππ* valence states are higher than in most of the other methods with the deviation being particularly large in comparison to the CASPT2 results. Nevertheless, a series of different methods, like MRCI [2, 4], EOM-CCSD [8], CC3 [3], and TDDFT [4] indicates that CASPT2 might be underestimating these transition energies. Therefore, we conclude that the current MRCI approach is adequate for calculation of vertical excitation energies.

Fig. 1 (around here)

3.2 Conical intersections

In Fig. 1 the MXS structures between ground state and the S_1 state are presented. The comparison of selected geometrical parameters for the ring-puckered (Fig. 1a) and the NH-stretched (Fig. 1b) MXS structures reveals that they are in very good agreement with the benchmark MRCI values [27].

In Fig. 1a, the MXS between the valence ππ* state and the ground state shows an out-of-plane deformation with strong stretching of one of the CN bonds. We shall refer to this conical intersection as the ring-puckered MXS. The values of dihedral CCCN and CCCH dihedral angles are very close to the benchmark ones, being only by ca. 2° smaller. The length of the broken CN bond is 1.607 Å, thus being 0.007 Å shorter than the value obtained with the benchmark method. In Fig. 1b, the NH-stretched MXS is shown. It arises from the crossing

For Peer Review Only

between the ground state and the lowest $\pi\sigma_{NH}$* state. In comparison to the benchmark MRCI value, the NH distance using the current method is shorter by 0.007 Å.

As mentioned in the Introduction, based on previous findings for other five-membered heteroaromatic molecules [30, 31, 33], we have searched for a planar ring-opened MXS in pyrrole as well. The optimized structure, obtained at the MRCI level of theory, is presented in Fig. 1c. It should be pointed out that the MXS is planar and that the CN distance is 2.512 Å, which is by about 0.9 Å longer than the CN distance observed in the ring puckered MXS (Fig. 1a). It is important to note that the ring-opened MXS is the lowest energy conical intersection identified in pyrrole so far and it arises from the crossing between the $\pi\sigma_{NC}$* state and the ground state.

Table 2. (around here)

Although the similarity of geometrical parameters suggests that the selected MR-CISD/SA-5-CASSCF(4,5)/BS level of theory is adequate, it is also of importance to compare the energies of the MXSs. MRCI and MRCI+Q energy values of pyrrole MXSs obtained by the MR-CISD(Q)/SA-5-CASSCF(4,5)/BS and benchmark MRCI values [27] are summarized in Table 2. The analysis of presented data shows that the energies of the MXSs are in very good agreement with the benchmark ones. The comparison among results reveals that the selected MRCI method is well suited for the description of both ring-puckering and NH-stretching mechanisms. In particular, the current MRCI and MRCI+Q energies of the ring-puckered MXS are by 0.06 eV higher and 0.07 eV lower than the benchmark MRCI and MRCI+Q values, respectively. For the NH-stretched MXS, the MRCI energy is by 0.04 eV higher, whereas the MRCI+Q value is by 0.18 eV lower than the benchmark values.

For Peer Review Only

3.3 Reaction paths

We have computed the reaction pathways between the ground state minimum and the three MXSs described in the previous section using the MR-CISD/SA-5-CASSCF(4,5)/BS level of theory. The resulting potential energy curves are shown in Fig. 2.

Fig. 2 (around here)

Comparison with the results obtained with the MR-CISD+Q/SA-5-CAS(6,5)+AUX(1)/d-aug-cc-pVDZ method (Fig. 2 in [27]) reveals that NH-stretching potential energy curves (Fig. 2a) agree very well for the ground state S_0 and the two Rydberg $^1A_2$ and $^1B_1$ states for the whole range of NH distances. The main difference is that the crossing between the lowest Rydberg state and the ground state occurs at around 1.9 Å in the present work instead of 2.1 Å found in our earlier study [27]. The other features of the potential energy curves exhibit the same behavior as observed earlier. Specifically, the lowest two Rydberg states show small energy barriers (0.24 eV for the $^1A_2$ state and 0.12 for the $^1B_1$ state) at the NH distance of 1.2 Å necessary to transform the π3s orbital into the $\pi\sigma_{NH}$* state as expected for a stretching of the NH bond. It should also be pointed out that the two valence $^1A_1$ and $^1B_2$ states show the same energy profile until the NH distance of 1.8 Å. After that, an intrusion of higher excited states occurs (not shown), which is presumably a direct consequence of the CAS(4,5) active space. However, in the NH stretching mechanism, the deactivation occurs via conical intersections among Rydberg states and the ground state and the differences in the valence states for large NH distances are of minor importance.

Fig. 2b shows that the LIIC path of the ring-puckering mechanism in the ππ* state occurs without barrier. Indeed, it is clearly seen that the lowest ππ* state is diabatically connected to the ground state, which may make it especially efficient for the internal conversion. The same result was observed in our previous study [27] thus providing additional

URL: http://mc.manuscriptcentral.com/tandf/tmph

For Peer Review Only

support for using the applied method. In the case of the ring-opening mechanism Fig. 2c shows that the initially excited ππ* states can deactivate without barrier along this pathway. The character of the state should, however, change into $\pi\sigma_{NC}$* in order to lead to the crossing with the ground state.

Apart from the fact that the NH-stretching mechanism should dominate at low excitation energies, it is difficult to draw general conclusions about the efficiency of each mechanism based on the reaction paths alone in a clear cut way. When the excitation leads into the spectral region of the ππ* state all mechanisms are energetically possible. In favor of the NH-stretching mechanism is the fact that it requires the smallest deformations from the Franck-Condon region in terms of mass-weighted distances (see Fig. 2). On the other hand, it also requires the diabatic transformation from the ππ* state into the $\pi\sigma_{NH}$* state, which depends upon the activation of out-of-plane modes [18, 27]. The ring-opening mechanism involves the lowest energy conical intersection, but it requires the largest deformations from the Franck-Condon region and diabatic changes in the wave function at the same time. Finally, the ring-puckering mechanism, as already mentioned, can directly proceed through a diabatic connection. However, it involves the highest energy portions of the seam of conical intersections.

4. Dynamics simulations of pyrrole

The non-adiabatic excited state dynamics of pyrrole was started from the S_4 state thus making all pathways discussed in the previous section energetically available. The resulting average adiabatic populations of the ground and excited states as a function of time are presented in Fig. 3. Their analysis shows that the S_4 state transfers its population to the S_3 state in the first 10 fs. After ca. 50 fs, the S_4 state is almost completely depopulated. The populations of S_3 and S_2 states reach a maximum at 10 fs and 20 fs, respectively. At about 75 fs, these states are

For Peer Review Only

already depopulated. The S_2 state shows a repopulation between 100 and 150 fs. The population of the S_1 state increases reaching a maximum at 75 fs. At 100 fs, the S_1 and S_0 states have approximately the same population. Between 100 fs and 200 fs, the simulation is basically reduced to the S_1/S_0 two-state dynamics, with the complete population transferred to the ground state at about 200 fs.

Fig. 3 (around here)

The S_1 population shows a consecutive two-step first order decay type of behavior. By fitting the S_1 population curve with the function

$$f(t) = \frac{\tau_2}{\tau_2 - \tau_1}\left[\exp\left(-\frac{t}{\tau_1}\right) - \exp\left(-\frac{t}{\tau_2}\right)\right], \qquad (1)$$

two time constants τ_1 = 44 ± 2 fs and τ_2 = 80 ± 2 fs are obtained. Here, τ_1 measures the population of S_1 from the collection of states S_4 to S_2 and τ_2 describes the depopulation $S_1 \rightarrow S_0$. The approximate time constant for the overall population of the ground state can be obtained by fitting the S_0 population with the function

$$f(t) = 1 - \exp\left(-\frac{t}{\tau_0}\right), \qquad (2)$$

which gives τ_0 = 139 ± 2 fs. Note that in these three time constants the error bars denote the uncertainty of the fitting procedure and not of the process itself, which certainly is larger than a few femtoseconds.

In Fig. 4 a summary of the results of the dynamics simulation in terms of the fraction of trajectories following each of the three mechanisms is given. The NH-stretching is the main mechanism after excitation of pyrrole to the S_4 state. This mechanism occurs in 80% of the trajectories. Other 13% follow ring-deformation mechanisms (ring-opening and ring-

URL: http://mc.manuscriptcentral.com/tandf/tmph

For Peer Review Only

puckering). 7% do not deactivate within the 200 fs of the dynamics simulation. Because of the uncertainties associated to the dynamics simulations and to the relatively small number of trajectories, these fractions should be taken as qualitative trends of occurrence of each mechanism, rather than a quantitative assessment of them. If trajectories starting in the ππ* and in the $\pi\sigma_{NH}$* states are independently analyzed, these fractions remain essentially the same, implying that the population of each mechanism depends on the excitation energy, but not on the nature of the state. The fact that the fast H atom is formed along the NH stretching pathway either excited in the ππ* or πσ* states has also been observed in the photofragment translational spectroscopy studies by Cronin et al. [26].

Experimental pump of pyrrole with 250 nm (4.96 eV) laser pulse followed by ionization probe with 241 nm (5.15 eV) pulse reveals two time constants, τ_f = 110 ± 80 fs and τ_s = 1100 ± 500 fs [19]. These time constants correspond to the time for formation of fast and slow H atoms, respectively. Since most of trajectories in our simulations finished in the ground state of the dissociated pyrrolyl + H system, the deactivation time τ_0 should also approximately give the time for the formation of the fast H atoms population. Indeed, the comparison of τ_0 and τ_f shows good agreement. Note, however, that the initial state in the experiments (low energy $\pi\sigma_{NH}$*) and in the simulations (high energy ππ* and $\pi\sigma_{NH}$*) are not the same. This is an indication that the fast H elimination occurs directly by the same process, as soon as there is enough energy to overcome the π3s/$\pi\sigma_{NH}$* barrier in the S_1 state.

Fig. 4 (around here)

Fig. 5 (around here)

The analysis of NH and CN bond distances was conducted for all trajectories and the results are presented in Fig. 5. The top panel of this figure shows that in some cases the CN distance is elongating during the dynamics. This behavior can be ascribed to the ring-opening

For Peer Review Only

and ring-puckering deactivation mechanisms. Since the main deactivation channel is the NH-stretching, the majority of trajectories do not exhibit elongation of this specific bond. In the bottom panel of Fig. 5 the NH distance is monitored. In this figure three kinds of trajectories can be distinguished. For part of the trajectories the NH distance remain constant at about 1 Å. They correspond to the trajectories following ring-distortion mechanisms. A minor fraction of trajectories (3) has the NH distance oscillating at a medium distance of about 2 or 3 Å. These are cases where the NH-stretching mechanism is activated, but instead finishing in dissociation, the hot ground state of pyrrole is formed. In most of the trajectories the NH distance is steadily increasing. In these cases, the NH-stretching mechanism is activated and the H atom elimination is taking place. It should be mentioned that a cut-off value of 10 Å for NH distance was used in Fig. 5 in order to simplify the data analysis. In some of the trajectories, however, the NH distance was longer, up to 40 Å.

Fig. 6 (around here)

Fig. 6a shows that the hydrogen dissociation starts on average 54 fs after the photoexcitation. The kinetic energy of the dissociated hydrogen atom has a broad distribution around the average value of 1.2 eV (Fig. 6b). This value is in very good agreement with the experimental results, ~1 eV [11, 26], for the center of the fast H-elimination peak in the kinetic energy release spectra. Note that, as expected, there is no formation of a slow H-elimination peak, which should take place in the picosecond timescale [19], much longer than the maximum simulation time (200 fs). The NH distance at the $S_1 \rightarrow S_0$ hopping time is shown in Fig. 6c for all trajectories that have returned to the ground state. The histogram shows two distinct peaks. The first peak with average at 1.0 Å will be discussed below. The second peak starts at 1.5 Å and presents a long tail for large distances up to 4 Å. This peak corresponds to the trajectories deactivated by means of the NH-stretching mechanism. Its average value at

For Peer Review Only

2.1 Å is 0.2 Å larger than the NH distance for the crossing between the lowest πσ* state and the ground state shown in Fig. 2 (left panel).

Fig. 7 (around here)

Twelve out of ninety trajectories did not follow the NH-stretching mechanism. They appear in the short-distance peak in Fig. 6c. In order to understand which kind of mechanism they followed, it is useful to project them on the Cremer-Pople (CP) space Q-ϕ. This is shown in Fig. 7 for all structures for which the S_1-S_0 energy gap is smaller than 0.5 eV (open dots) and for structures at the hopping time (full dots). The ring-opened MXS is at Q = 0 Å and the ring-puckered MXS is shown by a cross (E_1 conformation). Since the ring-opened and the ring-puckered conical intersections correspond to distinct types of structures on the crossing seam with different electronic configurations, it could be expected that the structures at the hopping time would cluster in two disjoint regions around these MXSs. This, however, is not the case. Fig. 7 shows that the non-adiabatic events occur in a large continuous portion of the CP space, indicating that the crossing seam spans this entire region. The degree of puckering varies from almost planar (Q = 0.15 Å) to the strongly puckered structures (Q = 0.75 Å). Most of hopping events occur at E_1, $^2T_1$ and ^2E conformations, indicating that not only the E_1 conformation of the ring-puckered MXS, but also other kinds of puckering can give rise to conical intersections in pyrrole.

If we take Q = 0.3 Å as an arbitrary threshold to distinguish between the ring-opening and ring-puckering mechanisms, nine trajectories deactivated at ring-puckered conformations and three trajectories deactivated at ring-opened conformations, thus corresponding to 10% and 3% of the total number of trajectories, respectively (see Fig. 4).

For Peer Review Only

5. Conclusions

The photochemical processes in pyrrole were investigated using a high-level multireference configuration interaction method (MRCI) giving a balanced description of the four studied excited states, two of Rydberg character and two valence states. Cuts along the potential energy surfaces connecting the Franck-Condon region and three different minima on the crossing seam (MXS) (NH dissociation, ring puckering, and a planar ring-opened MXS) describe possible deactivation pathways. One of these intersection points, the ring-opened MXS, was characterized for the first time. Although it is the conical intersection of the lowest energy identified in pyrrole so far, its efficiency for the internal conversion process seems to be reduced by the required strong geometric deformations and by the diabatic change of the initially excited $\pi\pi^*$ state into the $\pi\sigma_{NC}^*$ state, which in turn crosses the ground state.

Non-adiabatic surface-hopping dynamics simulations of pyrrole were performed for 200 fs starting in the S_4 state and using a high-level MR-CI approach for the electronic structure calculations. The dynamics simulations show that in fact all three types of conical intersections were accessed. The transfer of population from the initially excited S_4 state to the ground state takes place in about 140 fs. This process occurs basically in two steps, with the S_1 state being populated in about 44 fs and then being depleted in about 80 fs. Most of trajectories (80%) dissociated rapidly along the repulsive $\pi\sigma_{NH}^*$ state giving rise to a population of fast H atoms. The computed deactivation time of 140 fs agrees very well with the experimentally measured time constant of 110 fs for the formation of fast hydrogen atoms. The computed average kinetic energy agrees very well with the experimentally observed average kinetic energy of the fast hydrogen atoms. A fraction of 13% of trajectories follows ring-deformation channels involving either ring puckering (10%) or planar ring opening (3%). These fractions did not depend on whether the initial state had $\pi\pi^*$ or $\pi\sigma_{NH}^*$ character.

For Peer Review Only

Our calculations provide a detailed picture of the photodeactivation processes in pyrrole. Although the main objective of this work – the observation of the occurrence of the different deactivation mechanisms – has been accomplished, it should be noted that the participation of $\pi\sigma_{NH}$* states in the initial conditions was much higher than what would be expected from the oscillator strengths of these two transitions. This bias occurred because of the relatively high vertical excitation energy of the $^1B_1$ Rydberg state, which caused frequent exchange of position with the $\pi\pi$* in the Wigner sample. Interestingly, it turned out that the observed percentages of the different mechanisms was insensitive to the initial character of S_4, consequently implying that that this bias is not so critical for the general interpretations. Nevertheless, more investigations are needed to analyze the influence of excitation energies on the product yields in order to explain the experimentally observed strong energy dependence of the branching ratios for fast and slow hydrogen atoms.

Acknowledgments

This work was supported by the Austrian Science Fund within the framework of the Special Research Program F16 (Advanced Light Sources) and Project P18411-N19. The calculations were partially performed at the Linux PC cluster Schrödinger III of the computer center of the University of Vienna. The work in Zagreb (M.E.M and M.V.) was supported by the Ministry of Science, Education and Sport through the project 098-0982933-2920 and the COST D37 action.

References

[1] L. Serrano-Andrés, M. Merchán, I. Nebotgil, B. O. Roos, and M. Fulscher, J. Am. Chem. Soc. **115**, 6184 (1993).

[2] M. H. Palmer, I. C. Walker, and M. F. Guest, Chem. Phys. **238**, 179 (1998).

URL: http://mc.manuscriptcentral.com/tandf/tmph

For Peer Review Only

[3] O. Christiansen, J. Gauss, J. F. Stanton, and P. Jorgensen, J. Chem. Phys. **111**, 525 (1999).

[4] D. J. Tozer, R. D. Amos, N. C. Handy, B. O. Roos, and L. Serrano-Andres, Mol. Phys. **97**, 859 (1999).

[5] J. Wan, J. Meller, M. Hada, M. Ehara, and H. Nakatsuji, J. Chem. Phys. **113**, 7853 (2000).

[6] B. O. Roos, P. A. Malmqvist, V. Molina, L. Serrano-Andres, and M. Merchan, J. Chem. Phys. **116**, 7526 (2002).

[7] C. G. Zhan, and D. A. Dixon, J. Mol. Spectrosc. **216**, 81 (2002).

[8] P. Celani, and H. J. Werner, J. Chem. Phys. **119**, 5044 (2003).

[9] M. H. Palmer, and P. J. Wilson, Mol. Phys. **101**, 2391 (2003).

[10] M. Pastore, C. Angeli, and R. Cimiraglia, Chem. Phys. Lett. **422**, 522 (2006).

[11] D. A. Blank, S. W. North, and Y. T. Lee, Chem. Phys. **187**, 35 (1994).

[12] A. B. Trofimov, H. Köppel, and J. Schirmer, J. Chem. Phys. **109**, 1025 (1998).

[13] A. L. Sobolewski, W. Domcke, C. Dedonder-Lardeux, and C. Jouvet, PCCP **4**, 1093 (2002).

[14] J. Wei, A. Kuczmann, J. Riedel, F. Renth, and F. Temps, PCCP **5**, 315 (2003).

[15] V. Vallet, Z. G. Lan, S. Mahapatra, A. L. Sobolewski, and W. Domcke, Faraday Discuss. **127**, 283 (2004).

[16] V. Vallet, Z. G. Lan, S. Mahapatra, A. L. Sobolewski, and W. Domcke, J. Chem. Phys. **123** (2005).

[17] J. Wei, J. Riedel, A. Kuczmann, F. Renth, and F. Temps, Faraday Discuss. **127**, 267 (2004).

[18] H. Köppel, E. V. Gromov, and A. B. Trofimov, Chem. Phys. **304**, 35 (2004).

[19] H. Lippert, H. H. Ritze, I. V. Hertel, and W. Radloff, Chemphyschem **5**, 1423 (2004).

[20] A. J. van den Brom, M. Kapelios, T. N. Kitsopoulos, N. H. Nahler, B. Cronin, and M. N. R. Ashfold, PCCP **7**, 892 (2005).

[21] I. Frank, and K. Damianos, Journal of Chemical Physics **126** (2007).

For Peer Review Only

[22] Z. Lan, A. Dupays, V. Vallet, S. Mahapatra, and W. Domcke, Journal of Photochemistry and Photobiology a-Chemistry **190**, 177 (2007).

[23] Z. Lan, and W. Domcke, Chem. Phys. **350**, 125 (2008).

[24] A. Kumar, M. Kolaski, and K. S. Kim, J. Chem. Phys. **128** (2008).

[25] E. J. Shin, Bull. Korean Chem. Soc. **25**, 907 (2004).

[26] B. Cronin, M. G. D. Nix, R. H. Qadiri, and M. N. R. Ashfold, PCCP **6**, 5031 (2004).

[27] M. Barbatti, M. Vazdar, A. J. A. Aquino, M. Eckert-Maksic, and H. Lischka, J. Chem. Phys. **125**, 164323 (2006).

[28] V. Poterya, V. Profant, M. Farnik, P. Slavicek, and U. Buck, J. Chem. Phys. **127**, 064307 (2007).

[29] M. Barbatti, B. Sellner, A. J. A. Aquino, and H. Lischka, in *Radiation Induced Molecular Phenomena in Nucleic Acid*, edited by M. K. Shukla, and J. Leszczynski (Springer, Netherlands, 2008), pp. 209.

[30] S. Salzmann, M. Kleinschmidt, J. Tatchen, R. Weinkauf, and C. M. Marian, PCCP **10**, 380 (2008).

[31] N. Gavrilov, S. Salzmann, and C. M. Marian, Chem. Phys. **349**, 269 (2008).

[32] M. Barbatti, H. Lischka, S. Salzmann, and C. M. Marian, J. Chem. Phys., submitted (2008).

[33] S. Perun, A. L. Sobolewski, and W. Domcke, Chem. Phys. **313**, 107 (2005).

[34] M. Barbatti, and H. Lischka, J. Am. Chem. Soc. **130**, 6831 (2008).

[35] V. Profant, V. Poterya, M. Farnik, P. Slavicek, and U. Buck, J. Phys. Chem. A **111**, 12477 (2007).

[36] A. L. Sobolewski, and W. Domcke, Chem. Phys. **259**, 181 (2000).

[37] I. Antol, M. Vazdar, M. Barbatti, and M. Eckert-Maksic, Chem. Phys. **349**, 308 (2008).

[38] M. Barbatti, M. Ruckenbauer, J. J. Szymczak, A. J. A. Aquino, and H. Lischka, PCCP **10**, 482 (2008).

URL: http://mc.manuscriptcentral.com/tandf/tmph

For Peer Review Only

[39] J. C. Tully, Faraday Discuss. **110**, 407 (1998).

[40] A. Ferretti, G. Granucci, A. Lami, M. Persico, and G. Villani, J. Chem. Phys. **104**, 5517 (1996).

[41] N. L. Doltsinis, and D. Marx, Phys. Rev. Lett. **88**, 166402 (2002).

[42] M. Barbatti, G. Granucci, M. Persico, M. Ruckenbauer, M. Vazdar, M. Eckert-Maksic, and H. Lischka, J. Photochem. Photobiol., A **190**, 228 (2007).

[43] E. Fabiano, T. W. Keal, and W. Thiel, Chem. Phys. **349**, 334 (2008).

[44] J. Pittner, H. Lischka, and M. Barbatti, Chem. Phys., doi:10.1016/j.chemphys.2008.10.013 (2008).

[45] J. C. Tully, J. Chem. Phys. **93**, 1061 (1990).

[46] L. Sun, and W. L. Hase, in *Reviews in Computational Chemistry*, edited by K. B. Lipkowitz *et al.* (Wiley-VCH, New York, 2003), pp. 79.

[47] H. Lischka, R. Shepard, F. B. Brown, and I. Shavitt, Int. J. Quantum Chem. **S.15**, 91 (1981).

[48] H. Lischka, R. Shepard, R. M. Pitzer, I. Shavitt, M. Dallos, T. Müller, P. G. Szalay, M. Seth, G. S. Kedziora, S. Yabushita, and Z. Y. Zhang, PCCP **3**, 664 (2001).

[49] H. Lischka, R. Shepard, I. Shavitt, R. M. Pitzer, M. Dallos, T. Mueller, P. G. Szalay, F. B. Brown, R. Ahlrichs, H. J. Boehm, A. Chang, D. C. Comeau, R. Gdanitz, H. Dachsel, C. Ehrhardt, M. Ernzerhof, P. Hoechtl, S. Irle, G. Kedziora, T. Kovar, V. Parasuk, M. J. M. Pepper, P. Scharf, H. Schiffer, M. Schindler, M. Schueler, M. Seth, E. A. Stahlberg, J.-G. Zhao, S. Yabushita, Z. Zhang, M. Barbatti, S. Matsika, M. Schuurmann, D. R. Yarkony, S. R. Brozell, E. V. Beck, and J.-P. Blaudeau, COLUMBUS, an ab initio electronic structure program, release 5.9.1, www.univie.ac.at/columbus (2006).

[50] A. Bunge, J. Chem. Phys. **53**, 20 (1970).

[51] T. H. Dunning, J. Chem. Phys. **90**, 1007 (1989).

For Peer Review Only

[52] R. Shepard, H. Lischka, P. G. Szalay, T. Kovar, and M. Ernzerhof, J. Chem. Phys. **96**, 2085 (1992).

[53] R. Shepard, in *Modern Electronic Structure Theory*, edited by D. R. Yarkony (World Scientific, Singapore, 1995), p. 345.

[54] H. Lischka, M. Dallos, and R. Shepard, Mol. Phys. **100**, 1647 (2002).

[55] M. Dallos, H. Lischka, R. Shepard, D. R. Yarkony, and P. G. Szalay, Journal of Chemical Physics **120**, 7330 (2004).

[56] H. Lischka, M. Dallos, P. G. Szalay, D. R. Yarkony, and R. Shepard, Journal of Chemical Physics **120**, 7322 (2004).

[57] S. R. Langhoff, and E. R. Davidson, Int. J. Quantum Chem. **8**, 61 (1974).

[58] P. J. Bruna, S. D. Peyerimhoff, and R. J. Buenker, Chem. Phys. Lett. **72**, 278 (1980).

[59] V. Bonacic-Koutecky, and R. Mitric, Chem. Rev. **105**, 11 (2005).

[60] R. Mitric, V. Bonacic-Koutecky, J. Pittner, and H. Lischka, J. Chem. Phys. **125** (2006).

[61] W. C. Swope, H. C. Andersen, P. H. Berens, and K. R. Wilson, J. Chem. Phys. **76**, 637 (1982).

[62] G. Granucci, and M. Persico, J. Chem. Phys. **126**, 134114 (2007).

[63] D. Cremer, and J. A. Pople, J. Am. Chem. Soc. **97**, 1354 (1975).

[64] T. Helgaker, H. J. A. Jensen, P. Jørgensen, J. Olsen, K. Ruud, H. Ågren, T. Andersen, K. L. Bak, V. Bakken, O. Christiansen, P. Dahle, E. K. Dalskov, T. Enevoldsen, H. Heiberg, H. Hettema, D. Jonsson, S. Kirpekar, R. Kobayashi, H. Koch, K. V. Mikkelsen, P. Norman, M. J. Packer, T. Saue, P. R. Taylor, and O. Vahtras, DALTON, an ab initio electronic structure program, Release 1.0 (1997).

[65] M. Barbatti, G. Granucci, M. Ruckenbauer, M. Persico, and H. Lischka, NEWTON-X: a package for Newtonian dynamics close to the crossing seam, www.univie.ac.at/newtonx (2007).

For Peer Review Only

Tables

Table 1 – Vertical excitation energies of selected singlet states of pyrrole.

State		MRCI[a]	MRCI+Q[b]	TDDFT[c]	CASPT2	CC3[g]	Exp
S_0	$^1A_1$	0.00	0.00	0.00	0.00	0.00	
π3s	$^1A_2$	5.22	5.09	5.05	5.22[d]/5.22[e]	5.10	5.08[h]/5.22[i]
π3s	$^1B_1$	6.21	5.86	5.88	5.85[f]/5.92[e]	5.99	6.22[h]
ππ*	$^1A_1$	6.55	6.39	6.29	5.82[d]/5.98[e]	6.37	
ππ*	$^1B_2$	6.65	6.78	6.45	5.87[d]/5.95[e]	6.63	5.92[h]/6.2-6.4[i]

[a] Present results, MR-CISD/SA-5-CASSCF(4,5)/BS
[b] MR-CISD+Q/SA-5-CAS(6,5)+AUX(1)/d-aug-cc-pVDZ, Reference [27].
[c] Reference [4].
[d] Reference [6].
[e] Reference [8].
[f] Reference [1].
[g] Reference [3].
[h] Assigments given in Reference [9].
[i] Assigments given in Reference [3].

For Peer Review Only

Table 2 – Energy of pyrrole MXSs (in eV) relative to the minimum in the ground state.

MXS	MRCI[a]	MRCI+Q[a]	MRCI	MRCI+Q	MXS features
$\pi\pi^*/S_0$ (E_1)	4.95	4.86	4.89[b]	4.93[b]	ring puckering, Fig. 1a
$\pi\sigma_{NH}^*/S_0$	4.45	4.26	4.41[c]	4.44[c]	NH stretching, Fig. 1b
$\pi\sigma_{NC}^*/S_0$	4.11	3.86	-	-	ring opening, Fig. 1c

[a]Present results, MR-CISD/SA-5-CASSCF(4,5)/BS
[b]MR-CISD(Q)/SA-3-CAS(6,5) /6-31G(d), Reference [27].
[c]MR-CISD(Q)/SA-3-CAS(6,6)/6-31G(d), Reference [27].

For Peer Review Only

Figure Captions

Fig. 1. Structures and selected geometric parameters for pyrrole MXSs obtained at the MRCI level. Distances are given in Å and dihedral angles in degrees. The number in brackets correspond to the benchmark MRCI value from Ref. [27].

Fig. 2. Potential energy curves calculated at the MRCI level along a) the rigid NH-stretching coordinate and along the LIIC path from the ground state minimum to b) the ring-puckered MXS and to c) the ring-opened MXS.

Fig. 3. Average adiabatic populations of trajectories for each state as a function of time after initial photoexcitation of pyrrole into the S_4 state.

Fig. 4. Description and statistics of trajectory deactivation mechanisms.

Fig. 5. CN (top) and NH (bottom) distance variations as a function of time for all trajectories. The NH distance of 10 Å was used as a cut-off value (see text).

Fig. 6. Analysis of the trajectories showing NH dissociation. (a) Initial time of the dissociation, taking 2 Å for the NH bond as reference value. (b) Hydrogen kinetic energy. (c) NH distance for all trajectories at the time of the $S_1 \rightarrow S_0$ hopping.

Fig. 7. Distribution of conformations in the Cremer-Pople Q-ϕ space for trajectories following ring-deformation mechanisms. Full dots: conformations at the hopping time. Open dots: conformations with S_1-S_0 energy gaps smaller than 0.5 eV. Cross: ring puckered MXS.

For Peer Review Only

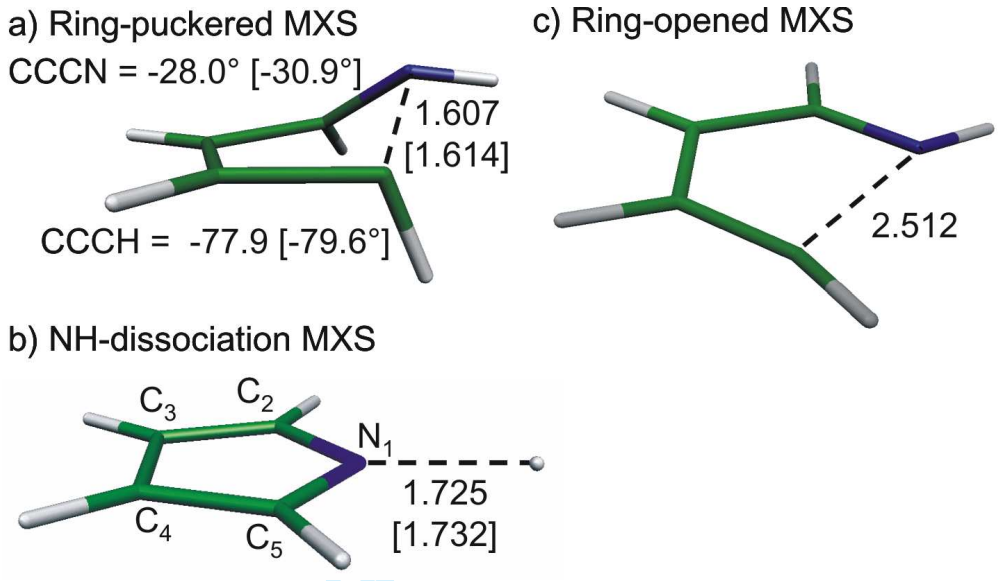

For Peer Review Only

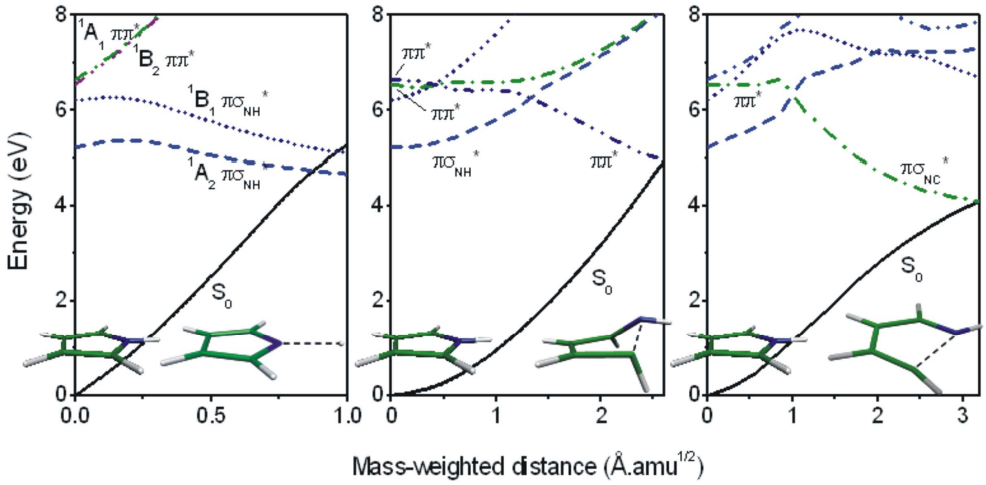

er Review Only

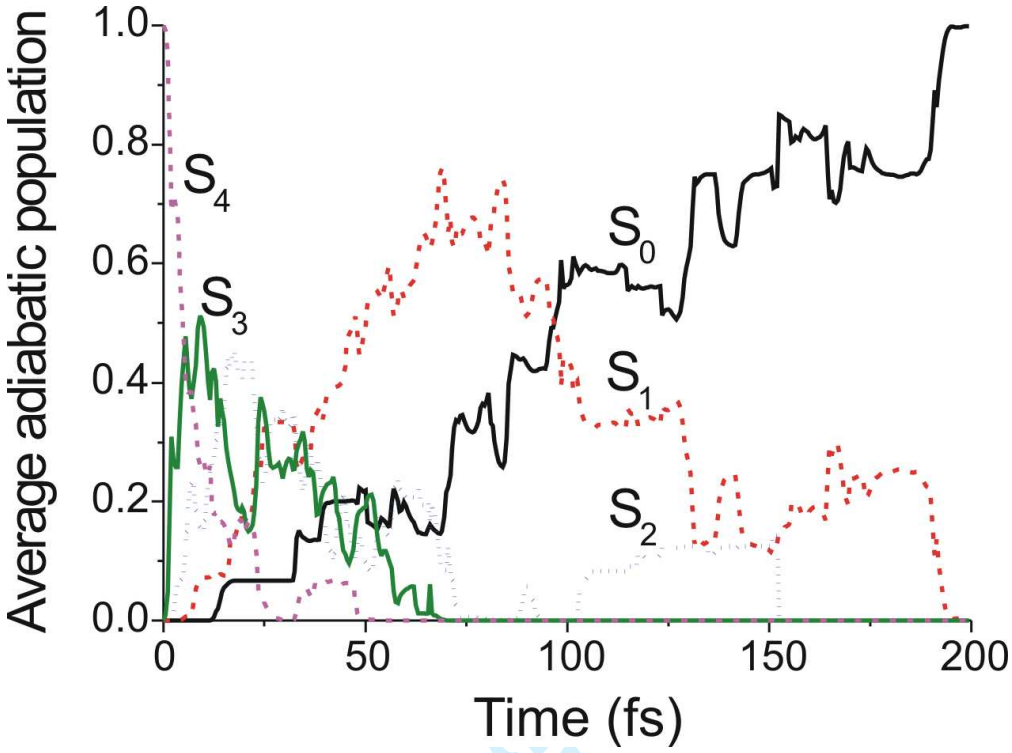

For Review Only

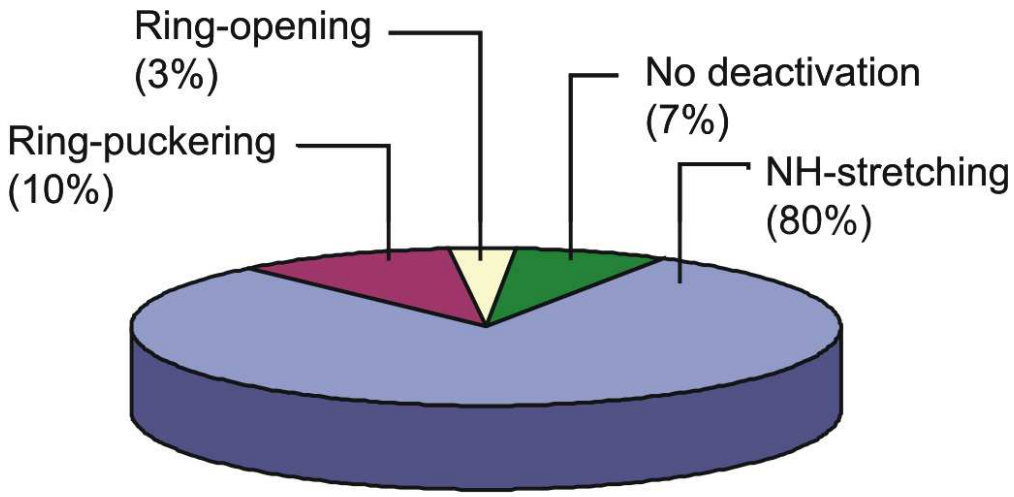

For Peer Review Only

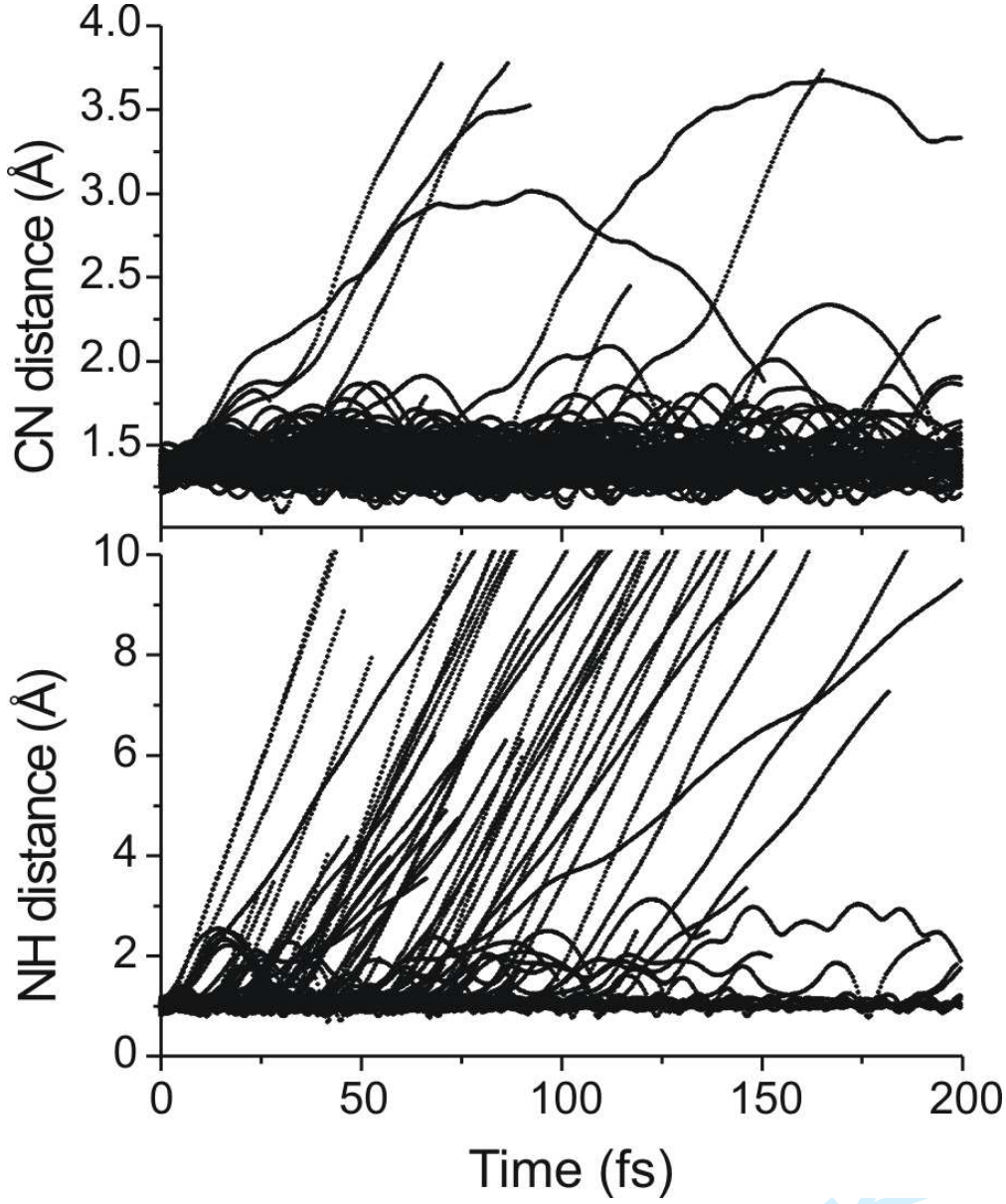
CN distance (Å)
4.0
3.5
3.0
2.5
2.0
1.5
NH distance (Å)
10
8
6
4
2
0
0
50
100
150
200
Time (fs)

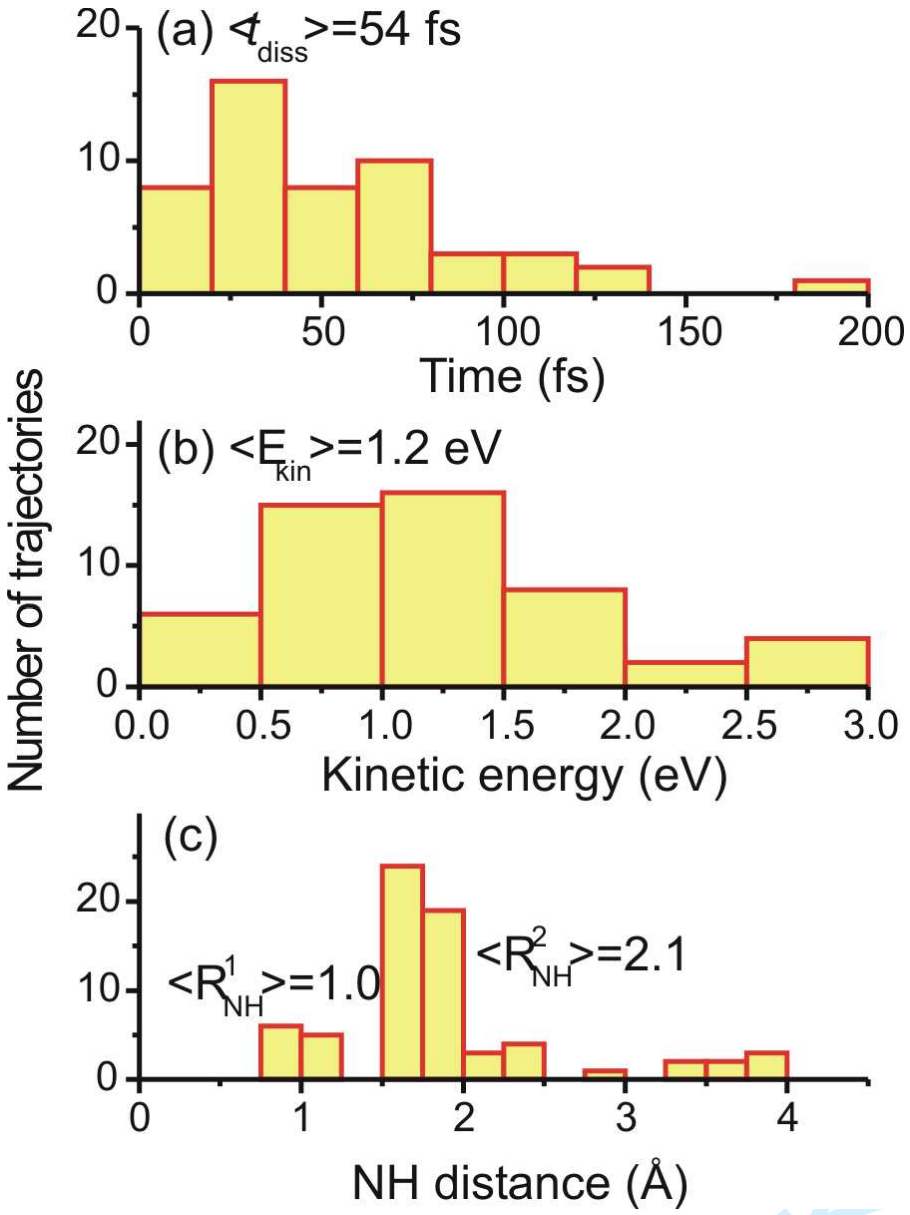
(a) <t_diss>=54 fs
Time (fs)
(b) <E_kin>=1.2 eV
Kinetic energy (eV)
Number of trajectories
(c)
<R^1_NH>=1.0
<R^2_NH>=2.1
NH distance (Å)

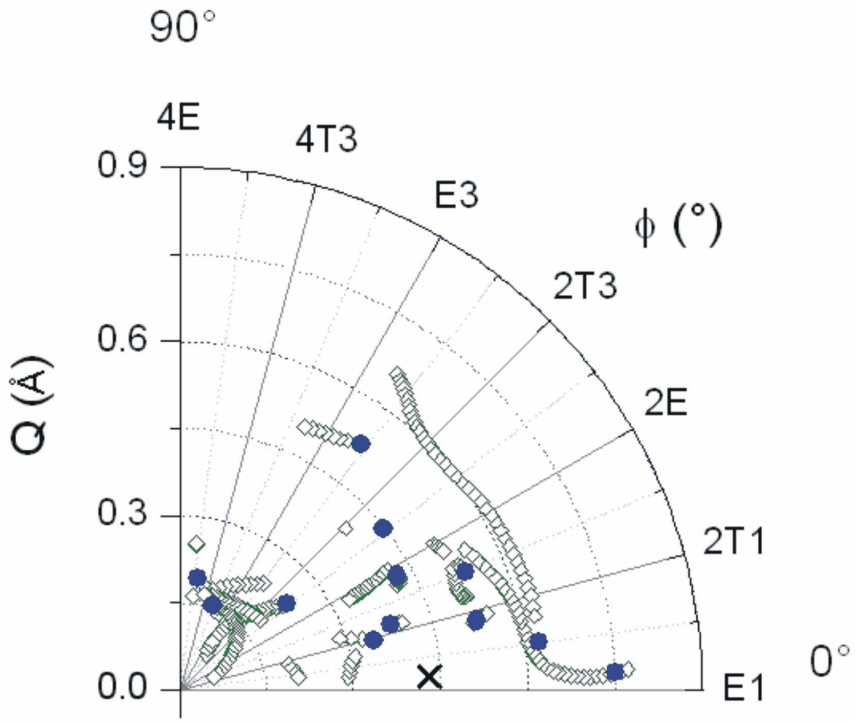

For Review Only

Excited-state non-adiabatic dynamics simulations of pyrrole

Mario Vazdar,[a] Mirjana Eckert-Maksić,[a*] Mario Barbatti,[b*] Hans Lischka[b*]

[a] *Laboratory for Physical-Organic Chemistry – Division of Organic Chemistry and Biochemistry. Rudjer Bošković Institute, 10002 Zagreb, Croatia;* [b] *Institute for Theoretical Chemistry – University of Vienna, Waehringerstrasse 17, A 1090 Vienna, Austria.*

For Peer Review Only

Abstract

Non-adiabatic on-the-fly-dynamics simulations of the photodynamics of pyrrole were performed at multireference configuration interaction level involving five electronic states with a simulation time of 200 fs. The analysis of the time dependence of the average state occupations shows that the deactivation of pyrrole to the electronic ground state takes place in about 140 fs. This deactivation time agrees very well with the experimentally measured time constant of 110 fs for the formation of fast hydrogen atoms. After excitation into the S_4 state, 80% of the trajectories followed the NH-stretching mechanism giving rise to a population of fast H atoms. The computed average kinetic energy is in good accord with the experimentally observed average kinetic energy of the fast hydrogen atoms. It is found that 10% of trajectories followed the ring-puckering mechanism and 3% followed the ring-opening mechanism. This latter mechanism was characterized in pyrrole for the first time and involves the conical intersection of lowest energy of this molecule.

Keywords: non-adiabatic dynamics; conical intersection; photochemistry; pyrrole

* Corresponding authors: H. Lischka (hans.lischka@univie.ac.at), M. Barbatti (mario.barbatti@univie.ac.at) and M. Eckert-Maksić (mmaksic@emma.irb.hr)

1. Introduction

Pyrrole is one of the simplest biologically relevant heteroaromatic compounds. For this reason, its electronic states have been intensively studied both experimentally and theoretically during the last decades with the emphasis on its UV spectrum [1-10] and its photodynamics [11-24]. In particular, it is known that the deactivation of UV-excited pyrrole to the ground state occurs at a very short (femtosecond) time scale [19] with low luminescence quantum yields [25], indicating the dominance of internal conversion processes. Sobolewski and coworkers [13] have proposed that the deactivation of pyrrole and related heteroatomic compounds occurs via the NH-stretching mechanism along a $^1\pi\sigma_{NH}^*$ repulsive state. This mechanism, which has been examined in detail [15, 16, 22, 23] by means of wave packet dynamics simulations, can fully explain the presence of fast H atoms in the photofragmentation spectra [26]. Nevertheless, the mechanism responsible for the formation of slow H atoms and of other experimentally observed fragments such as HCN and CNH_2 [11, 14, 17, 19, 20] is still subject of considerable debate [15, 19, 26-28].

Recently, we have suggested [27] that non-adiabatic deactivation of pyrrole may also proceed via a ring-puckering mechanism. This second kind of mechanism could not only be the source of heavy fragments, but also partially explain the slow H atoms [29]. Also recently, a third deactivation mechanism that can be relevant for pyrrole was identified in thiophene [30], furan [31], imidazole [32], and in the imidazole group of adenine [33]. In this mechanism the deactivation of five-membered rings proceeds by a planar ring-opening deformation. This process was observed to occur in a minor fraction of trajectories during dynamics simulations of adenine [34]. Based on these findings, we have currently attempted and succeeded to locate this type of mechanism in pyrrole, too.

For Peer Review Only

Profant *et al*. [35] and Poterya *et al.* [28] have experimentally investigated the photolysis of pyrrole clusters. In addition, they have also performed theoretical calculations on the isolated pyrrole and on pyrrole complexes [28]. They have found that in presence of solvent molecules the NH stretching mechanism is inhibited, which results in a strong reduction of the fast H atom elimination process while keeping the slow H atom elimination. These are important results that on one hand once more confirm the role of the NH-stretching mechanism for the fast H atoms formation and on the other hand indicate that ring deformation mechanisms should be involved in the slow H atoms formation.

The strong dependence of different fragment yields on the excitation energy [26] indicates that the individual mechanisms are in mutual competition and can play different roles depending on the initial conditions. Excited-state energy surfaces have been investigated in detail under special consideration of crossings between different energy surfaces as already mentioned above [1, 18, 23, 27, 28, 36] and reaction paths have been constructed subsequently. This information led to substantial progress in the understanding of the photochemical processes in pyrrole. However, it turned out to be very difficult to estimate the importance of individual intersections and related reaction pathways. In order to better understand how these mechanisms are activated, it is desirable to perform dynamics simulations. Such simulations exhibit a substantial complexity. For instance, as for selecting the proper quantum chemical methods, it needs to be taken into account that: first, the non-adiabatic dynamics of pyrrole involves multiple excited states showing often multireference character and, secondly, that it is essentially impossible to identify just a few important internal degrees of freedom by which the photochemical reaction mechanism can be described. Therefore, an essential condition is the usage of the full set of nuclear coordinates. These are usual requirements to be met e.g. in simulations of organic chromophores exhibiting high density of excited states [34, 37, 38]. One convenient way to satisfy especially

URL: http://mc.manuscriptcentral.com/tandf/tmph

For Peer Review Only

the second condition is to use mixed-quantum classical dynamics methods [39-44]. In this work surface hopping dynamics is performed using the fewest-switches algorithm of Tully [45]. The advantage of this approach is that it allows the application of an "on-the-fly" strategy [42, 43, 46] where a pre-selection of certain internal degrees of freedom and any fitting of pre-computed potential energy points is avoided by computing at each time step the energies, the complete energy gradient and non-adiabatic coupling terms required for the integration of Newton's equations of motion and the time-dependent Schrödinger equation. This on-the-fly strategy is computationally very expensive and requires analytical energy gradients and non-adiabatic coupling vectors for computational efficiency. Due to the stringent computational requirements most of the photodynamical simulations have been performed so far at the relatively cost-effective complete active space self consistent field level (CASSCF). Since in this case dynamical electron correlation effects are mostly neglected, the relative balance of electronic states of different character can be strongly violated. It should be stressed that the non-adiabatic dynamics simulations presented here were carried out at a significantly higher level using the MR-CISD method including five electronic states. This represents the state-of-the-art approach for this kind of simulations, which has not been documented before for molecules of the size of pyrrole to the best of our knowledge. The present calculations have been made possible by use of the analytic gradient features of the program package COLUMBUS [47-49] as it will be described below.

2. Computational details

Multireference configuration interaction (MRCI) and complete active space self-consistent field (CASSCF) calculations were performed for pyrrole. The CAS space was comprised of four π electrons in five orbitals (two π orbitals, two π* orbitals and one Rydberg 3s orbital). This space will be conventionally designated as CAS(4,5) in the text. State averaging was

URL: http://mc.manuscriptcentral.com/tandf/tmph

For Peer Review Only

performed over five singlet states with equal weights (ground state, two valence ππ* states and two Rydberg π3s states), which will be denoted as SA-5. MRCI calculations were performed based on the orbitals computed by the SA-5-CASSCF(4,5) wave function. The reference configurations for the MRCI were constructed within the CAS(4,5) by allowing single and double excitations from the two π orbitals into the two π* orbitals and the Rydberg 3s orbital. The final configuration space was constructed by allowing all single and double excitations from the reference configurations into the virtual orbital space (MR-CISD). All core electrons and the lowest eight additional orbitals were frozen in the MRCI calculations and the interacting space restriction [50] was applied. The basis set was composed of aug'-cc-pVDZ type [51] on the nitrogen and carbon atoms (the prime indicates that d-aug functions were removed). On the hydrogen atom connected to nitrogen, the cc-pVDZ basis set was used, whereas for the remaining hydrogen atoms the cc'-pVDZ basis set was used (the prime signifies that p-functions were deleted). This hybrid basis set will be denoted as BS.

The MRCI approach and the basis set were selected by balancing the accuracy requirements of the calculations of four excited states of different character (see Table 1) and the need for computational efficiency, since an on-the-fly approach requires several tens of thousands of individual MRCI calculations to be carried out. Therefore, before starting the dynamics simulations an extensive set of calculations had been performed, including the Franck-Condon region, the seam of conical intersections, and reaction pathways. For the determination of minima on the crossing seam (MXS), starting geometries were selected from our previous MRCI calculations on pyrrole [27] and were reoptimized with the above-described MRCI method. Reaction paths for the two ring-deformation processes were constructed by the method of linear interpolation of internal coordinates (LIIC) between the ground-state geometry and the corresponding ring-deformed conical intersections. The reaction path for the NH-stretching process was constructed by rigidly stretching the NH

For Peer Review Only

distance in steps of 0.2 Å starting from the ground state equilibrium structure up to a NH distance of 2.6 Å.

All energy calculations and MXS optimizations were performed by using analytical gradient and non-adiabatic coupling procedures described in References [52-56]. For vertical excitation energy calculations, the Davidson correction (+Q) [53, 57, 58] was used in order to describe higher order excitation effects. For the C_{2v} labeling of the states, the *x* axis was assumed to be oriented perpendicular to the ring plane.

Mixed quantum-classical dynamics calculations were performed for pyrrole by using an on-the-fly approach [42, 43, 46, 59, 60]. Energies, gradients, and non-adiabatic coupling vectors were computed at each time step at the MR-CISD/SA-5-CASSCF(4,5)/BS level of theory. The nuclear motion was represented by classical trajectories computed by numerical integration of Newton's equations by the velocity-Verlet algorithm [61]. Non-adiabatic effects were taken into account by means of the surface hopping approach [45]. Time-dependent adiabatic populations were corrected for decoherence effects [62] (α = 0.1 hartree) and used to calculate surface hopping probabilities in accordance to the Tully's fewest switches approach [45]. In order to alleviate the computational costs, no coupling vectors were calculated between non-consecutive states [44]. In total, 90 trajectories were computed. The initial Cartesian coordinates and momenta were selected from a quantum harmonic oscillator (Wigner) distribution in the ground state. The trajectories were started in the S_4 state at these geometries. This procedure gave rise to a composition of 60% of trajectories initially in the $\pi\pi^*$ states and 40% in the $\pi 3s/\pi\sigma_{NH}^*$ states. The minimum excitation energy was 6.36 eV while the average was 6.76 eV with a standard deviation of 0.26 eV. The trajectories were then propagated for a maximum time of 200 fs with a time step of 0.5 fs.

The structures of the puckered geometries were described in terms of the Cremer-Pople parameters Q and ϕ [63]. While the parameter Q measures the extent of puckering (Q =

For Peer Review Only

0 Å indicates a planar structure), the parameter ϕ describes the kind of puckering. For 5-mebered rings, there are only few kinds of puckered conformations available: envelope conformations with atom *k* above (^{k}E) or below (E$_{k}$) the ring plane and twisted conformations with atom *k* above the ring plane and atom *k*-1 below the ring plane (^{k}T$_{k-1}$). Because of the pyrrole symmetry, ϕ can be reduced to the 0° – 90° range by projecting all values on this quadrant.

All CASSCF and MR-CISD+Q calculations were performed with the COLUMBUS [47-49] program package. The atomic orbital (AO) integrals and AO gradient integrals have been calculated with program modules taken from DALTON [64]. The dynamic simulations were carried out using the NEWTON-X program [42, 65] with an interface to the COLUMBUS program package.

Table 1. (around here)

3. Analysis of the energy surfaces

In order to investigate the reliability of the MRCI method used in the dynamics study, we have performed a series of tests and comparisons with other previously published results. Specifically, we have compared vertical excitation energies, reaction paths, and MXS structures with results obtained with methods of higher level of theory.

3.1 Vertical excitation energies

The theoretical computation of vertical excitation energies of pyrrole and the assignment of the experimental UV spectrum have been a matter of discussion for a long period of time [1, 3, 4, 8, 9]. The currently calculated values are compared to other available theoretical and experimental results in Table 1. The comparison reveals that vertical excitation energies computed by the MR-CISD/SA-5-CASSCF(4,5)/BS method are in good accordance with

For Peer Review Only

results obtained previously by the MR-CISD+Q/SA-5-CAS(6,5)+AUX(1)/d-aug-cc-pVDZ method [27] where the auxiliary (AUX) orbital represents the 3s Rydberg orbital into which single excitations from the valence CAS(6,5) are allowed. Most of the calculated vertical excitation energies differ by ca. 0.1-0.2 eV, except in the case of the $^1B_1$ state where this difference is 0.35 eV. Furthermore, the present results for the $^1A_2$ and $^1B_1$ Rydberg states are in excellent agreement with experimental values assigned in Ref. [9]. The current energies of the ππ* valence states are higher than in most of the other methods with the deviation being particularly large in comparison to the CASPT2 results. Nevertheless, a series of different methods, like MRCI [2, 4], EOM-CCSD [8], CC3 [3], and TDDFT [4] indicates that CASPT2 might be underestimating these transition energies. Therefore, we conclude that the current MRCI approach is adequate for calculation of vertical excitation energies.

Fig. 1 (around here)

3.2 Conical intersections

In Fig. 1 the MXS structures between ground state and the S_1 state are presented. The comparison of selected geometrical parameters for the ring-puckered (Fig. 1a) and the NH-stretched (Fig. 1b) MXS structures reveals that they are in very good agreement with the benchmark MRCI values [27].

In Fig. 1a, the MXS between the valence ππ* state and the ground state shows an out-of-plane deformation with strong stretching of one of the CN bonds. We shall refer to this conical intersection as the ring-puckered MXS. The values of dihedral CCCN and CCCH dihedral angles are very close to the benchmark ones, being only by ca. 2° smaller. The length of the broken CN bond is 1.607 Å, thus being 0.007 Å shorter than the value obtained with the benchmark method. In Fig. 1b, the NH-stretched MXS is shown. It arises from the crossing

For Peer Review Only

between the ground state and the lowest $\pi\sigma_{NH}^*$ state. In comparison to the benchmark MRCI value, the NH distance using the current method is shorter by 0.007 Å.

As mentioned in the Introduction, based on previous findings for other five-membered heteroaromatic molecules [30, 31, 33], we have searched for a planar ring-opened MXS in pyrrole as well. The optimized structure, obtained at the MRCI level of theory, is presented in Fig. 1c. It should be pointed out that the MXS is planar and that the CN distance is 2.512 Å, which is by about 0.9 Å longer than the CN distance observed in the ring puckered MXS (Fig. 1a). It is important to note that the ring-opened MXS is the lowest energy conical intersection identified in pyrrole so far and it arises from the crossing between the $\pi\sigma_{NC}^*$ state and the ground state.

Table 2. (around here)

Although the similarity of geometrical parameters suggests that the selected MR-CISD/SA-5-CASSCF(4,5)/BS level of theory is adequate, it is also of importance to compare the energies of the MXSs. MRCI and MRCI+Q energy values of pyrrole MXSs obtained by the MR-CISD(Q)/SA-5-CASSCF(4,5)/BS and benchmark MRCI values [27] are summarized in Table 2. The analysis of presented data shows that the energies of the MXSs are in very good agreement with the benchmark ones. The comparison among results reveals that the selected MRCI method is well suited for the description of both ring-puckering and NH-stretching mechanisms. In particular, the current MRCI and MRCI+Q energies of the ring-puckered MXS are by 0.06 eV higher and 0.07 eV lower than the benchmark MRCI and MRCI+Q values, respectively. For the NH-stretched MXS, the MRCI energy is by 0.04 eV higher, whereas the MRCI+Q value is by 0.18 eV lower than the benchmark values.

For Peer Review Only

3.3 Reaction paths

We have computed the reaction pathways between the ground state minimum and the three MXSs described in the previous section using the MR-CISD/SA-5-CASSCF(4,5)/BS level of theory. The resulting potential energy curves are shown in Fig. 2.

Fig. 2 (around here)

Comparison with the results obtained with the MR-CISD+Q/SA-5-CAS(6,5)+AUX(1)/d-aug-cc-pVDZ method (Fig. 2 in [27]) reveals that NH-stretching potential energy curves (Fig. 2a) agree very well for the ground state S_0 and the two Rydberg $^1A_2$ and $^1B_1$ states for the whole range of NH distances. The main difference is that the crossing between the lowest Rydberg state and the ground state occurs at around 1.9 Å in the present work instead of 2.1 Å found in our earlier study [27]. The other features of the potential energy curves exhibit the same behavior as observed earlier. Specifically, the lowest two Rydberg states show small energy barriers (0.24 eV for the $^1A_2$ state and 0.12 for the $^1B_1$ state) at the NH distance of 1.2 Å necessary to transform the π3s orbital into the $\pi\sigma_{NH}$* state as expected for a stretching of the NH bond. It should also be pointed out that the two valence $^1A_1$ and $^1B_2$ states show the same energy profile until the NH distance of 1.8 Å. After that, an intrusion of higher excited states occurs (not shown), which is presumably a direct consequence of the CAS(4,5) active space. However, in the NH stretching mechanism, the deactivation occurs via conical intersections among Rydberg states and the ground state and the differences in the valence states for large NH distances are of minor importance.

Fig. 2b shows that the LIIC path of the ring-puckering mechanism in the ππ* state occurs without barrier. Indeed, it is clearly seen that the lowest ππ* state is diabatically connected to the ground state, which may make it especially efficient for the internal conversion. The same result was observed in our previous study [27] thus providing additional

URL: http://mc.manuscriptcentral.com/tandf/tmph

For Peer Review Only

support for using the applied method. In the case of the ring-opening mechanism Fig. 2c shows that the initially excited ππ* states can deactivate without barrier along this pathway. The character of the state should, however, change into $\pi\sigma_{NC}$* in order to lead to the crossing with the ground state.

Apart from the fact that the NH-stretching mechanism should dominate at low excitation energies, it is difficult to draw general conclusions about the efficiency of each mechanism based on the reaction paths alone in a clear cut way. When the excitation leads into the spectral region of the ππ* state all mechanisms are energetically possible. In favor of the NH-stretching mechanism is the fact that it requires the smallest deformations from the Franck-Condon region in terms of mass-weighted distances (see Fig. 2). On the other hand, it also requires the diabatic transformation from the ππ* state into the $\pi\sigma_{NH}$* state, which depends upon the activation of out-of-plane modes [18, 27]. The ring-opening mechanism involves the lowest energy conical intersection, but it requires the largest deformations from the Franck-Condon region and diabatic changes in the wave function at the same time. Finally, the ring-puckering mechanism, as already mentioned, can directly proceed through a diabatic connection. However, it involves the highest energy portions of the seam of conical intersections.

4. Dynamics simulations of pyrrole

The non-adiabatic excited state dynamics of pyrrole was started from the S_4 state thus making all pathways discussed in the previous section energetically available. The resulting average adiabatic populations of the ground and excited states as a function of time are presented in Fig. 3. Their analysis shows that the S_4 state transfers its population to the S_3 state in the first 10 fs. After ca. 50 fs, the S_4 state is almost completely depopulated. The populations of S_3 and S_2 states reach a maximum at 10 fs and 20 fs, respectively. At about 75 fs, these states are

For Peer Review Only

already depopulated. The S_2 state shows a repopulation between 100 and 150 fs. The population of the S_1 state increases reaching a maximum at 75 fs. At 100 fs, the S_1 and S_0 states have approximately the same population. Between 100 fs and 200 fs, the simulation is basically reduced to the S_1/S_0 two-state dynamics, with the complete population transferred to the ground state at about 200 fs.

Fig. 3 (around here)

The S_1 population shows a consecutive two-step first order decay type of behavior. By fitting the S_1 population curve with the function

$$f(t) = \frac{\tau_2}{\tau_2 - \tau_1}\left[\exp\left(-\frac{t}{\tau_1}\right) - \exp\left(-\frac{t}{\tau_2}\right)\right], \qquad (1)$$

two time constants τ_1 = 44 ± 2 fs and τ_2 = 80 ± 2 fs are obtained. Here, τ_1 measures the population of S_1 from the collection of states S_4 to S_2 and τ_2 describes the depopulation $S_1 \rightarrow S_0$. The approximate time constant for the overall population of the ground state can be obtained by fitting the S_0 population with the function

$$f(t) = 1 - \exp\left(-\frac{t}{\tau_0}\right), \qquad (2)$$

which gives τ_0 = 139 ± 2 fs. Note that in these three time constants the error bars denote the uncertainty of the fitting procedure and not of the process itself, which certainly is larger than a few femtoseconds.

In Fig. 4 a summary of the results of the dynamics simulation in terms of the fraction of trajectories following each of the three mechanisms is given. The NH-stretching is the main mechanism after excitation of pyrrole to the S_4 state. This mechanism occurs in 80% of the trajectories. Other 13% follow ring-deformation mechanisms (ring-opening and ring-

URL: http://mc.manuscriptcentral.com/tandf/tmph

For Peer Review Only

puckering). 7% do not deactivate within the 200 fs of the dynamics simulation. Because of the uncertainties associated to the dynamics simulations and to the relatively small number of trajectories, these fractions should be taken as qualitative trends of occurrence of each mechanism, rather than a quantitative assessment of them. If trajectories starting in the $\pi\pi^*$ and in the $\pi\sigma_{NH}^*$ states are independently analyzed, these fractions remain essentially the same, implying that the population of each mechanism depends on the excitation energy, but not on the nature of the state. The fact that the fast H atom is formed along the NH stretching pathway either excited in the $\pi\pi^*$ or $\pi\sigma^*$ states has also been observed in the photofragment translational spectroscopy studies by Cronin et al. [26].

Experimental pump of pyrrole with 250 nm (4.96 eV) laser pulse followed by ionization probe with 241 nm (5.15 eV) pulse reveals two time constants, $\tau_f = 110 \pm 80$ fs and $\tau_s = 1100 \pm 500$ fs [19]. These time constants correspond to the time for formation of fast and slow H atoms, respectively. Since most of trajectories in our simulations finished in the ground state of the dissociated pyrrolyl + H system, the deactivation time τ_0 should also approximately give the time for the formation of the fast H atoms population. Indeed, the comparison of τ_0 and τ_f shows good agreement. Note, however, that the initial state in the experiments (low energy $\pi\sigma_{NH}^*$) and in the simulations (high energy $\pi\pi^*$ and $\pi\sigma_{NH}^*$) are not the same. This is an indication that the fast H elimination occurs directly by the same process, as soon as there is enough energy to overcome the $\pi 3s/\pi\sigma_{NH}^*$ barrier in the S_1 state.

Fig. 4 (around here)

Fig. 5 (around here)

The analysis of NH and CN bond distances was conducted for all trajectories and the results are presented in Fig. 5. The top panel of this figure shows that in some cases the CN distance is elongating during the dynamics. This behavior can be ascribed to the ring-opening

For Peer Review Only

and ring-puckering deactivation mechanisms. Since the main deactivation channel is the NH-stretching, the majority of trajectories do not exhibit elongation of this specific bond. In the bottom panel of Fig. 5 the NH distance is monitored. In this figure three kinds of trajectories can be distinguished. For part of the trajectories the NH distance remain constant at about 1 Å. They correspond to the trajectories following ring-distortion mechanisms. A minor fraction of trajectories (3) has the NH distance oscillating at a medium distance of about 2 or 3 Å. These are cases where the NH-stretching mechanism is activated, but instead finishing in dissociation, the hot ground state of pyrrole is formed. In most of the trajectories the NH distance is steadily increasing. In these cases, the NH-stretching mechanism is activated and the H atom elimination is taking place. It should be mentioned that a cut-off value of 10 Å for NH distance was used in Fig. 5 in order to simplify the data analysis. In some of the trajectories, however, the NH distance was longer, up to 40 Å.

Fig. 6 (around here)

Fig. 6a shows that the hydrogen dissociation starts on average 54 fs after the photoexcitation. The kinetic energy of the dissociated hydrogen atom has a broad distribution around the average value of 1.2 eV (Fig. 6b). This value is in very good agreement with the experimental results, ~1 eV [11, 26], for the center of the fast H-elimination peak in the kinetic energy release spectra. Note that, as expected, there is no formation of a slow H-elimination peak, which should take place in the picosecond timescale [19], much longer than the maximum simulation time (200 fs). The NH distance at the $S_1 \rightarrow S_0$ hopping time is shown in Fig. 6c for all trajectories that have returned to the ground state. The histogram shows two distinct peaks. The first peak with average at 1.0 Å will be discussed below. The second peak starts at 1.5 Å and presents a long tail for large distances up to 4 Å. This peak corresponds to the trajectories deactivated by means of the NH-stretching mechanism. Its average value at

URL: http://mc.manuscriptcentral.com/tandf/tmph

For Peer Review Only

2.1 Å is 0.2 Å larger than the NH distance for the crossing between the lowest πσ* state and the ground state shown in Fig. 2 (left panel).

Fig. 7 (around here)

Twelve out of ninety trajectories did not follow the NH-stretching mechanism. They appear in the short-distance peak in Fig. 6c. In order to understand which kind of mechanism they followed, it is useful to project them on the Cremer-Pople (CP) space Q-ϕ. This is shown in Fig. 7 for all structures for which the S_1-S_0 energy gap is smaller than 0.5 eV (open dots) and for structures at the hopping time (full dots). The ring-opened MXS is at Q = 0 Å and the ring-puckered MXS is shown by a cross (E_1 conformation). Since the ring-opened and the ring-puckered conical intersections correspond to distinct types of structures on the crossing seam with different electronic configurations, it could be expected that the structures at the hopping time would cluster in two disjoint regions around these MXSs. This, however, is not the case. Fig. 7 shows that the non-adiabatic events occur in a large continuous portion of the CP space, indicating that the crossing seam spans this entire region. The degree of puckering varies from almost planar (Q = 0.15 Å) to the strongly puckered structures (Q = 0.75 Å). Most of hopping events occur at E_1, $^2T_1$ and ^2E conformations, indicating that not only the E_1 conformation of the ring-puckered MXS, but also other kinds of puckering can give rise to conical intersections in pyrrole.

If we take Q = 0.3 Å as an arbitrary threshold to distinguish between the ring-opening and ring-puckering mechanisms, nine trajectories deactivated at ring-puckered conformations and three trajectories deactivated at ring-opened conformations, thus corresponding to 10% and 3% of the total number of trajectories, respectively (see Fig. 4).

For Peer Review Only

5. Conclusions

The photochemical processes in pyrrole were investigated using a high-level multireference configuration interaction method (MRCI) giving a balanced description of the four studied excited states, two of Rydberg character and two valence states. Cuts along the potential energy surfaces connecting the Franck-Condon region and three different minima on the crossing seam (MXS) (NH dissociation, ring puckering, and a planar ring-opened MXS) describe possible deactivation pathways. One of these intersection points, the ring-opened MXS, was characterized for the first time. Although it is the conical intersection of the lowest energy identified in pyrrole so far, its efficiency for the internal conversion process seems to be reduced by the required strong geometric deformations and by the diabatic change of the initially excited $\pi\pi^*$ state into the $\pi\sigma_{NC}^*$ state, which in turn crosses the ground state.

Non-adiabatic surface-hopping dynamics simulations of pyrrole were performed for 200 fs starting in the S_4 state and using a high-level MR-CI approach for the electronic structure calculations. The dynamics simulations show that in fact all three types of conical intersections were accessed. The transfer of population from the initially excited S_4 state to the ground state takes place in about 140 fs. This process occurs basically in two steps, with the S_1 state being populated in about 44 fs and then being depleted in about 80 fs. Most of trajectories (80%) dissociated rapidly along the repulsive $\pi\sigma_{NH}^*$ state giving rise to a population of fast H atoms. The computed deactivation time of 140 fs agrees very well with the experimentally measured time constant of 110 fs for the formation of fast hydrogen atoms. The computed average kinetic energy agrees very well with the experimentally observed average kinetic energy of the fast hydrogen atoms. A fraction of 13% of trajectories follows ring-deformation channels involving either ring puckering (10%) or planar ring opening (3%). These fractions did not depend on whether the initial state had $\pi\pi^*$ or $\pi\sigma_{NH}^*$ character.

For Peer Review Only

Our calculations provide a detailed picture of the photodeactivation processes in pyrrole. Although the main objective of this work – the observation of the occurrence of the different deactivation mechanisms – has been accomplished, it should be noted that the participation of $\pi\sigma_{NH}^*$ states in the initial conditions was much higher than what would be expected from the oscillator strengths of these two transitions. This bias occurred because of the relatively high vertical excitation energy of the $^1B_1$ Rydberg state, which caused frequent exchange of position with the $\pi\pi^*$ in the Wigner sample. Interestingly, it turned out that the observed percentages of the different mechanisms was insensitive to the initial character of S_4, consequently implying that that this bias is not so critical for the general interpretations. Nevertheless, more investigations are needed to analyze the influence of excitation energies on the product yields in order to explain the experimentally observed strong energy dependence of the branching ratios for fast and slow hydrogen atoms.

Acknowledgments

This work was supported by the Austrian Science Fund within the framework of the Special Research Program F16 (Advanced Light Sources) and Project P18411-N19. The calculations were partially performed at the Linux PC cluster Schrödinger III of the computer center of the University of Vienna. The work in Zagreb (M.E.M and M.V.) was supported by the Ministry of Science, Education and Sport through the project 098-0982933-2920 and the COST D37 action.

References

[1] L. Serrano-Andrés, M. Merchán, I. Nebotgil, B. O. Roos, and M. Fulscher, J. Am. Chem. Soc. **115**, 6184 (1993).

[2] M. H. Palmer, I. C. Walker, and M. F. Guest, Chem. Phys. **238**, 179 (1998).

URL: http://mc.manuscriptcentral.com/tandf/tmph

For Peer Review Only

[3] O. Christiansen, J. Gauss, J. F. Stanton, and P. Jorgensen, J. Chem. Phys. **111**, 525 (1999).

[4] D. J. Tozer, R. D. Amos, N. C. Handy, B. O. Roos, and L. Serrano-Andres, Mol. Phys. **97**, 859 (1999).

[5] J. Wan, J. Meller, M. Hada, M. Ehara, and H. Nakatsuji, J. Chem. Phys. **113**, 7853 (2000).

[6] B. O. Roos, P. A. Malmqvist, V. Molina, L. Serrano-Andres, and M. Merchan, J. Chem. Phys. **116**, 7526 (2002).

[7] C. G. Zhan, and D. A. Dixon, J. Mol. Spectrosc. **216**, 81 (2002).

[8] P. Celani, and H. J. Werner, J. Chem. Phys. **119**, 5044 (2003).

[9] M. H. Palmer, and P. J. Wilson, Mol. Phys. **101**, 2391 (2003).

[10] M. Pastore, C. Angeli, and R. Cimiraglia, Chem. Phys. Lett. **422**, 522 (2006).

[11] D. A. Blank, S. W. North, and Y. T. Lee, Chem. Phys. **187**, 35 (1994).

[12] A. B. Trofimov, H. Köppel, and J. Schirmer, J. Chem. Phys. **109**, 1025 (1998).

[13] A. L. Sobolewski, W. Domcke, C. Dedonder-Lardeux, and C. Jouvet, PCCP **4**, 1093 (2002).

[14] J. Wei, A. Kuczmann, J. Riedel, F. Renth, and F. Temps, PCCP **5**, 315 (2003).

[15] V. Vallet, Z. G. Lan, S. Mahapatra, A. L. Sobolewski, and W. Domcke, Faraday Discuss. **127**, 283 (2004).

[16] V. Vallet, Z. G. Lan, S. Mahapatra, A. L. Sobolewski, and W. Domcke, J. Chem. Phys. **123** (2005).

[17] J. Wei, J. Riedel, A. Kuczmann, F. Renth, and F. Temps, Faraday Discuss. **127**, 267 (2004).

[18] H. Köppel, E. V. Gromov, and A. B. Trofimov, Chem. Phys. **304**, 35 (2004).

[19] H. Lippert, H. H. Ritze, I. V. Hertel, and W. Radloff, Chemphyschem **5**, 1423 (2004).

[20] A. J. van den Brom, M. Kapelios, T. N. Kitsopoulos, N. H. Nahler, B. Cronin, and M. N. R. Ashfold, PCCP **7**, 892 (2005).

[21] I. Frank, and K. Damianos, Journal of Chemical Physics **126** (2007).

For Peer Review Only

[22] Z. Lan, A. Dupays, V. Vallet, S. Mahapatra, and W. Domcke, Journal of Photochemistry and Photobiology a-Chemistry **190**, 177 (2007).

[23] Z. Lan, and W. Domcke, Chem. Phys. **350**, 125 (2008).

[24] A. Kumar, M. Kolaski, and K. S. Kim, J. Chem. Phys. **128** (2008).

[25] E. J. Shin, Bull. Korean Chem. Soc. **25**, 907 (2004).

[26] B. Cronin, M. G. D. Nix, R. H. Qadiri, and M. N. R. Ashfold, PCCP **6**, 5031 (2004).

[27] M. Barbatti, M. Vazdar, A. J. A. Aquino, M. Eckert-Maksic, and H. Lischka, J. Chem. Phys. **125**, 164323 (2006).

[28] V. Poterya, V. Profant, M. Farnik, P. Slavicek, and U. Buck, J. Chem. Phys. **127**, 064307 (2007).

[29] M. Barbatti, B. Sellner, A. J. A. Aquino, and H. Lischka, in *Radiation Induced Molecular Phenomena in Nucleic Acid*, edited by M. K. Shukla, and J. Leszczynski (Springer, Netherlands, 2008), pp. 209.

[30] S. Salzmann, M. Kleinschmidt, J. Tatchen, R. Weinkauf, and C. M. Marian, PCCP **10**, 380 (2008).

[31] N. Gavrilov, S. Salzmann, and C. M. Marian, Chem. Phys. **349**, 269 (2008).

[32] M. Barbatti, H. Lischka, S. Salzmann, and C. M. Marian, J. Chem. Phys., submitted (2008).

[33] S. Perun, A. L. Sobolewski, and W. Domcke, Chem. Phys. **313**, 107 (2005).

[34] M. Barbatti, and H. Lischka, J. Am. Chem. Soc. **130**, 6831 (2008).

[35] V. Profant, V. Poterya, M. Farnik, P. Slavicek, and U. Buck, J. Phys. Chem. A **111**, 12477 (2007).

[36] A. L. Sobolewski, and W. Domcke, Chem. Phys. **259**, 181 (2000).

[37] I. Antol, M. Vazdar, M. Barbatti, and M. Eckert-Maksic, Chem. Phys. **349**, 308 (2008).

[38] M. Barbatti, M. Ruckenbauer, J. J. Szymczak, A. J. A. Aquino, and H. Lischka, PCCP **10**, 482 (2008).

URL: http://mc.manuscriptcentral.com/tandf/tmph

For Peer Review Only

[39] J. C. Tully, Faraday Discuss. **110**, 407 (1998).

[40] A. Ferretti, G. Granucci, A. Lami, M. Persico, and G. Villani, J. Chem. Phys. **104**, 5517 (1996).

[41] N. L. Doltsinis, and D. Marx, Phys. Rev. Lett. **88**, 166402 (2002).

[42] M. Barbatti, G. Granucci, M. Persico, M. Ruckenbauer, M. Vazdar, M. Eckert-Maksic, and H. Lischka, J. Photochem. Photobiol., A **190**, 228 (2007).

[43] E. Fabiano, T. W. Keal, and W. Thiel, Chem. Phys. **349**, 334 (2008).

[44] J. Pittner, H. Lischka, and M. Barbatti, Chem. Phys., doi:10.1016/j.chemphys.2008.10.013 (2008).

[45] J. C. Tully, J. Chem. Phys. **93**, 1061 (1990).

[46] L. Sun, and W. L. Hase, in *Reviews in Computational Chemistry*, edited by K. B. Lipkowitz *et al.* (Wiley-VCH, New York, 2003), pp. 79.

[47] H. Lischka, R. Shepard, F. B. Brown, and I. Shavitt, Int. J. Quantum Chem. **S.15**, 91 (1981).

[48] H. Lischka, R. Shepard, R. M. Pitzer, I. Shavitt, M. Dallos, T. Müller, P. G. Szalay, M. Seth, G. S. Kedziora, S. Yabushita, and Z. Y. Zhang, PCCP **3**, 664 (2001).

[49] H. Lischka, R. Shepard, I. Shavitt, R. M. Pitzer, M. Dallos, T. Mueller, P. G. Szalay, F. B. Brown, R. Ahlrichs, H. J. Boehm, A. Chang, D. C. Comeau, R. Gdanitz, H. Dachsel, C. Ehrhardt, M. Ernzerhof, P. Hoechtl, S. Irle, G. Kedziora, T. Kovar, V. Parasuk, M. J. M. Pepper, P. Scharf, H. Schiffer, M. Schindler, M. Schueler, M. Seth, E. A. Stahlberg, J.-G. Zhao, S. Yabushita, Z. Zhang, M. Barbatti, S. Matsika, M. Schuurmann, D. R. Yarkony, S. R. Brozell, E. V. Beck, and J.-P. Blaudeau, COLUMBUS, an ab initio electronic structure program, release 5.9.1, www.univie.ac.at/columbus (2006).

[50] A. Bunge, J. Chem. Phys. **53**, 20 (1970).

[51] T. H. Dunning, J. Chem. Phys. **90**, 1007 (1989).

For Peer Review Only

[52] R. Shepard, H. Lischka, P. G. Szalay, T. Kovar, and M. Ernzerhof, J. Chem. Phys. **96**, 2085 (1992).

[53] R. Shepard, in *Modern Electronic Structure Theory*, edited by D. R. Yarkony (World Scientific, Singapore, 1995), p. 345.

[54] H. Lischka, M. Dallos, and R. Shepard, Mol. Phys. **100**, 1647 (2002).

[55] M. Dallos, H. Lischka, R. Shepard, D. R. Yarkony, and P. G. Szalay, Journal of Chemical Physics **120**, 7330 (2004).

[56] H. Lischka, M. Dallos, P. G. Szalay, D. R. Yarkony, and R. Shepard, Journal of Chemical Physics **120**, 7322 (2004).

[57] S. R. Langhoff, and E. R. Davidson, Int. J. Quantum Chem. **8**, 61 (1974).

[58] P. J. Bruna, S. D. Peyerimhoff, and R. J. Buenker, Chem. Phys. Lett. **72**, 278 (1980).

[59] V. Bonacic-Koutecky, and R. Mitric, Chem. Rev. **105**, 11 (2005).

[60] R. Mitric, V. Bonacic-Koutecky, J. Pittner, and H. Lischka, J. Chem. Phys. **125** (2006).

[61] W. C. Swope, H. C. Andersen, P. H. Berens, and K. R. Wilson, J. Chem. Phys. **76**, 637 (1982).

[62] G. Granucci, and M. Persico, J. Chem. Phys. **126**, 134114 (2007).

[63] D. Cremer, and J. A. Pople, J. Am. Chem. Soc. **97**, 1354 (1975).

[64] T. Helgaker, H. J. A. Jensen, P. Jørgensen, J. Olsen, K. Ruud, H. Ågren, T. Andersen, K. L. Bak, V. Bakken, O. Christiansen, P. Dahle, E. K. Dalskov, T. Enevoldsen, H. Heiberg, H. Hettema, D. Jonsson, S. Kirpekar, R. Kobayashi, H. Koch, K. V. Mikkelsen, P. Norman, M. J. Packer, T. Saue, P. R. Taylor, and O. Vahtras, DALTON, an ab initio electronic structure program, Release 1.0 (1997).

[65] M. Barbatti, G. Granucci, M. Ruckenbauer, M. Persico, and H. Lischka, NEWTON-X: a package for Newtonian dynamics close to the crossing seam, www.univie.ac.at/newtonx (2007).

For Peer Review Only

Tables

Table 1 – Vertical excitation energies of selected singlet states of pyrrole.

State		MRCI[a]	MRCI+Q[b]	TDDFT[c]	CASPT2	CC3[g]	Exp
S_0	$^1A_1$	0.00	0.00	0.00	0.00	0.00	
$\pi 3s$	$^1A_2$	5.22	5.09	5.05	5.22[d]/5.22[e]	5.10	5.08[h]/5.22[i]
$\pi 3s$	$^1B_1$	6.21	5.86	5.88	5.85[f]/5.92[e]	5.99	6.22[h]
$\pi\pi^*$	$^1A_1$	6.55	6.39	6.29	5.82[d]/5.98[e]	6.37	
$\pi\pi^*$	$^1B_2$	6.65	6.78	6.45	5.87[d]/5.95[e]	6.63	5.92[h]/6.2-6.4[i]

[a] Present results, MR-CISD/SA-5-CASSCF(4,5)/BS
[b] MR-CISD+Q/SA-5-CAS(6,5)+AUX(1)/d-aug-cc-pVDZ, Reference [27].
[c] Reference [4].
[d] Reference [6].
[e] Reference [8].
[f] Reference [1].
[g] Reference [3].
[h] Assigments given in Reference [9].
[i] Assigments given in Reference [3].

For Peer Review Only

Table 2 – Energy of pyrrole MXSs (in eV) relative to the minimum in the ground state.

MXS	MRCI[a]	MRCI+Q[a]	MRCI	MRCI+Q	MXS features
$\pi\pi^*/S_0$ (E_1)	4.95	4.86	4.89[b]	4.93[b]	ring puckering, Fig. 1a
$\pi\sigma_{NH}^*/S_0$	4.45	4.26	4.41[c]	4.44[c]	NH stretching, Fig. 1b
$\pi\sigma_{NC}^*/S_0$	4.11	3.86	-	-	ring opening, Fig. 1c

[a]Present results, MR-CISD/SA-5-CASSCF(4,5)/BS
[b]MR-CISD(Q)/SA-3-CAS(6,5) /6-31G(d), Reference [27].
[c]MR-CISD(Q)/SA-3-CAS(6,6)/6-31G(d), Reference [27].

For Peer Review Only

Figure Captions

Fig. 1. Structures and selected geometric parameters for pyrrole MXSs obtained at the MRCI level. Distances are given in Å and dihedral angles in degrees. The number in brackets correspond to the benchmark MRCI value from Ref. [27].

Fig. 2. Potential energy curves calculated at the MRCI level along a) the rigid NH-stretching coordinate and along the LIIC path from the ground state minimum to b) the ring-puckered MXS and to c) the ring-opened MXS.

Fig. 3. Average adiabatic populations of trajectories for each state as a function of time after initial photoexcitation of pyrrole into the S_4 state.

Fig. 4. Description and statistics of trajectory deactivation mechanisms.

Fig. 5. CN (top) and NH (bottom) distance variations as a function of time for all trajectories. The NH distance of 10 Å was used as a cut-off value (see text).

Fig. 6. Analysis of the trajectories showing NH dissociation. (a) Initial time of the dissociation, taking 2 Å for the NH bond as reference value. (b) Hydrogen kinetic energy. (c) NH distance for all trajectories at the time of the $S_1 \rightarrow S_0$ hopping.

Fig. 7. Distribution of conformations in the Cremer-Pople Q-ϕ space for trajectories following ring-deformation mechanisms. Full dots: conformations at the hopping time. Open dots: conformations with S_1-S_0 energy gaps smaller than 0.5 eV. Cross: ring puckered MXS.

For Peer Review Only